

The Antarctic stratospheric Nitrogen Hole: Southern Hemisphere and Antarctic springtime total nitrogen dioxide and total ozone variability as observed in Sentinel-5p TROPOMI data

Adrianus de Laat, Jos van Geffen, Piet Stammes, Ronald van der A, Henk Eskes and J. Pepijn Veefkind

5 Royal Netherlands Meteorological Institute (KNMI), De Bilt, The Netherlands

Correspondence: Adrianus de Laat (laatdej@knmi.nl)

Abstract.

Denitrification of the stratospheric vortex is a crucial process for the Antarctic Ozone Hole formation resulting in an analogous stratospheric “Nitrogen Hole”. Here, 2018-2021 daily TROPOMI measurements are used for the first time for a detailed characterization of this Nitrogen Hole. Nitrogen dioxide total columns exhibit strong spatiotemporal and seasonal variations associated with both photochemistry as well as transport and mixing processes. Combined with total ozone column data two main regimes are identified: inner-vortex ozone and nitrogen dioxide depleted air and outer-vortex air enhanced in ozone and nitrogen dioxide. Within the vortex total ozone and total stratospheric nitrogen dioxide are strongly correlated which is much less evident outside of the vortex. Connecting both main regimes are what is defined here as “mixing lines”, a third regime of coherent patterns in the total nitrogen dioxide column - total ozone column phase space. These mixing lines exist because of differences in three dimensional variations of nitrogen dioxide and ozone thereby providing information about vortex dynamics and cross-vortex edge mixing. On the other hand, interannual variability of nitrogen dioxide – total ozone characteristics are rather small except in 2019 when the vortex was unusually unstable. Overall, the results show that daily stratospheric nitrogen dioxide column satellite measurements provide an innovative means for characterizing polar stratospheric denitrification processes, vortex dynamics and potentially long term monitoring if the total nitrogen column data record is extended with past satellite observations.

1. Introduction

Stratospheric nitrogen plays a crucial role in the formation of the Antarctic ozone hole. The hole forms during Antarctic springtime when halogens - mostly chlorine but also some bromine - are massively released from stable reservoir species like ClONO₂, HOCl and HCl (Solomon, 1990; Solomon and Keys, 1992; Dessler, 2000; von Clarmann, 2013). Extremely low stratospheric temperatures during Antarctic winter after formation of the stratospheric polar vortex result in widespread formation of small particles containing nitrogen oxides – so-called Polar Stratospheric Clouds (PSC) – which slowly sediment. This process depletes nitrogen oxides (denitrification/denoxification) in the Antarctic stratospheric vortex (Farman

et al., 1985; Solomon and Garcia, 1983; Salawitch et al., 1989; Fahey et al., 1990; Tabazadeh et al., 2000; Weimer, 2022).

30 The presence of the stratospheric polar vortex prevents resupply of nitrogen oxides from outside the vortex. The return of sunlight to the Antarctic stratosphere during Antarctic spring to the denitrified polar stratosphere leads to the formation of halogen radicals (Solomon et al., 1999; Santee et al., 2008; Strahan et al., 2014). The lack of nitrogen oxides – combined with the presence of PSCs – allows the halogen radicals to catalytically destroy ozone and thus cause the rapid formation of the Antarctic Ozone Hole (Hurwitz et al., 2015). Stratospheric ozone depletion ceases either when all ozone is destroyed or if

35 the stratosphere becomes warm enough and unfavorable for PSCs allowing for the re-formation of halogen reservoir species like HCl (Müller et al., 2008; Strahan et al., 2018; Stone et al., 2021). The warming in turn is caused by increasing sunlight and absorption of that sunlight but sometimes also by stratospheric vortex instability.

The ozone depleted Antarctic stratospheric vortex is easily identified in for example satellite measurements of the total ozone column (TCO₃). It is characterized by a large gradient of ozone rich outer-vortex air and O₃ depleted inner vortex air.

40 This gradient is not only present in O₃ but also in other trace gases like nitrogen oxides, as outlined and pioneered by John F. Noxon in the late 1970s (Noxon, 1978; 1979). This cliff-like large vortex edge trace gas gradient (Schoeberl et al., 1992; Joseph and Lagras, 2002; Waugh and Polvani et al., 2010) is therefore referred to as “the Noxon cliff”. The presence of this cliff reflects air masses on either side of the cliff with very different chemical histories (Dirksen et al., 2011).

Studying Noxon cliff characteristics for a long time depended on numerical modelling (*e.g.* Solomon and Garcia, 1983; Toon et al., 1987; Garcia and Solomon, 1994; Struthers et al., 2004), ground based observations (*e.g.* Gil and Cacho, 1992; Solomon et al., 1993; Kondo et al., 1994; Sanders et al., 1999; Struthers et al., 2004; Bortoli et al., 2005; Yela et al., 2005; Cook and Roscoe, 2009) and aircraft or balloon measurement campaigns over Antarctica (*e.g.* Goldman et al., 1978; Pommereau and Goutail, 1988; Fahey et al., 1989).

45

The advance of new innovative satellite instruments from the middle 1990s onwards but especially after 2000 enabled exploration of new approaches for monitoring the Antarctic Noxon cliff (Bodeker et al., 2002; Ricaud et al., 2005; Manney et al., 2006; Sato et al., 2009). The use of satellite observations for studying (mostly Antarctic) polar stratospheric nitrogen compounds and the Noxon Cliff has been predominantly done with satellite limb observations (*e.g.* Callis et al., 1983; Mount et al., 1994; Rinsland et al., 1996; Haley et al., 2004; Funke et al., 2005; von Savigny et al., 2005; Butz et al., 2006; Davies et al., 2006; Kerzenmacher et al., 2008; Köhl et al., 2008; Kritten et al., 2010; Bourassa et al., 2011; Khosrawi et al., 2011; Sofieva et al., 2012; Belmonte Rivas et al., 2014; Khosrawi et al., 2017; Dubé et al., 2020; Strode et al., 2022). Note that

50 many of these papers only touch upon the Noxon cliff, *i.e.* it is seen in the measurements and presented as an example of the observational capacity of a certain satellite and/or data product. Some results have been reported on the use of nitrogen dioxide (NO₂) total columns/stratospheric columns for nadir looking satellites but without a focus on polar regions (Belmonte Rivas et al., 2014; Beirle et al., 2016). Note that a main interest in stratospheric or total NO₂ from nadir-viewing

60 satellites is because of the need to remove the stratospheric component from total column amounts to arrive at the tropospheric NO₂ column (*e.g.* Hilboll et al., 2013).

There are a few research publications that touch upon satellite nadir total or stratospheric nitrogen dioxide (NO₂) observations over polar regions. Wenig et al. (2004) explore satellite nadir total stratospheric NO₂ (SNO₂) column measurements from the GOME instrument. They identify the Noxon cliff in Arctic springtime observations in 1997 in relation to the Arctic stratospheric vortex which persisted much longer than typical during that year. However, they do not explore the Antarctic region for similar purposes even though they mention multiple times that the Noxon cliff is present in both polar regions and that denitrification is larger over Antarctica relative to the Arctic. Richter et al. (2005) also explores GOME observations of total column O₃ (TCO₃), total NO₂ (TNO₂) as well as OCIO over Antarctica during the early 2000s with a focus on the well-known September 2002 Antarctic vortex split (Ricaud et al., 2005; Richter et al., 2005; von Savigny et al., 2005; Yela et al., 2005). They observe strongly reduced inner vortex SNO₂ during early Antarctic spring that largely vanished after the vortex split. However, no effort is put into quantitatively correlating TNO₂/SNO₂ with TCO₃ and/or OCIO. Adams et al. (2013) explore some OMI TNO₂ data and TCO₃ data in their study of ground-based observations at the Eureka station in northern Canada in relation to the anomalous longevity of the 2011 Arctic stratospheric vortex. They observe enhanced NO₂ and O₃ when outer-vortex air passes over Eureka associated with photochemical NO₂ production and the stratospheric vortex preventing mixing of outer-vortex air with inner-vortex air, causing NO₂ and O₃ rich stratospheric air to accumulate in the region bordering the Antarctic stratospheric vortex. They also show the conjunction of NO₂ and O₃ depleted inner-vortex air in OMI data but do not analyze those observations in more detail. Gordon et al. (2020) explore OMI TNO₂ and TCO₃ in relation to (upper) stratospheric and mesospheric NO_x formation due to energetic particle precipitation (EEP) but do not explore OMI TNO₂ beyond that application. The Noxon cliff has also been identified satellite nadir observations of nitrous acid (HNO₃) total columns of the European IASI satellite (Wespes et al., 2009, 2022; Ronsmans et al., 2016) as removal of HNO₃ from the Antarctic stratosphere is part of the denitrification process. Those studies showed that – not unexpectedly – Antarctic stratospheric vortex stability was important for inner-vortex HNO₃ and the strength of the Noxon cliff. However, in-depth analysis of the Noxon cliff in IASI HNO₃ observations is still also lacking. Note that strong cross-vortex gradients have also been observed in nadir viewing satellite measurements of OCIO (Kühl et al., 2006, 2008; Oetjen et al., 2011; Puķīte et al., 2021; Pinardi et al., 2022)

Satellite-observation-based exploration of the Noxon cliff and the denitrification process thus has almost exclusively been restricted to limb-sounding type satellite. Insofar as can be assessed the use of satellite nadir NO₂ measurements for in-depth studying the Antarctic stratosphere and denitrification has been absent. Even exploitation of the IASI HNO₃ data for this purpose has remained limited – in part also because of the need to average IASI HNO₃ data to reach sufficient data accuracy.

The TROPospheric Monitoring Instrument (TROPOMI) is the first of the next generation of hyperspectral UV/VIS satellite instruments. Designed and developed based on experience with satellite instruments like GOME, SCIAMACHY, GOME and GOME-2 it provides satellite observations of unprecedented spatial resolution and accuracy. Although developed for monitoring tropospheric pollution, total NO₂ column measurements from TROPOMI allows for studying stratospheric NO₂ as well since the entire Southern Hemisphere south of approximately 45° S – and thus Antarctica – is

devoid of large NO₂ sources. Antarctica is effectively unpopulated and combined with a moratorium on industrial mining activities emissions associated with combustion are largely missing. Without much vegetated land, soil NO_x emission are small and although little is known about the occurrence of lightning near Antarctic the atmospheric conditions do not favor widespread frequent occurrence of lightning. NO_x production due to nitrate photolysis in the Antarctic snowpack is too small
100 to yield tropospheric column amounts measurable by TROPOMI (France et al., 2011; Frey et al., 2013, 2015; Barbero et al., 2021). NO₂ emissions from the largest known single point source in Antarctic – the active volcano Mt. Erebus (Oppenheimer et al., 2005) – are likewise too small to affect NO_x columns on a continental scale. Hence, TNO₂ at high southern latitudes is dominated by SNO₂ columns. There thus is every reason to start exploring TROPOMI TNO₂ or SNO₂ over Antarctica – where they are nearly each other’s equivalent - to characterize the Noxon Cliff for NO₂ as well as the
105 denitrification/denoxification process.

Furthermore, the current suite of satellites that can be used for stratospheric monitoring is aging and the number of such satellites is dwindling. This is a significant concern for the scientific community and their commitment towards monitoring the ozone layer as part of the Montreal Protocol for “Protection of the Ozone Layer”. Recovery due to the phase out of emissions of ozone depleting substances is a slow process and full recovery is only expected in the second half of the 21st
110 century. However, unusual stratospheric events can strongly affect the ozone layer thickness from year to year. Whether such year-to-year changes in stratospheric ozone are anomalous or the result of natural variability is crucial for confident statements whether recovery is progressing as expected (or not). Satellite instrument measuring the stratospheric chemical composition other than ozone have been essential for understanding this year-to-year variability and thus meeting the commitment of the scientific community towards monitoring the ozone layer support of the Montreal Protocol. Given the
115 aging suite of stratospheric monitoring satellites and their dwindling numbers, identifying new stratospheric monitoring applications is more than welcome for continued stratospheric monitoring. Especially if these applications are based on satellite instruments that are planned to remain available for many decades into the future.

This paper presents the first steps towards assessing high spatial resolution daily TROPOMI TNO₂ and SNO₂ Southern Hemisphere middle and high latitude measurements and in particular its relationship with TCO₃. First, the TROPOMI SNO₂
120 measurements are evaluated by comparison with ground based southern hemisphere and Antarctic SNO₂ column observations. Daily and multi-day TROPOMI TNO₂ measurements are then explored to characterize their spatiotemporal distribution and variability over and around Antarctica during local springtime. Subsequently daily TROPOMI SNO₂ column measurements are collocated with daily TCO₃ data. Similarities and differences in spatiotemporal distributions of both TROPOMI SNO₂ and TCO₃ are identified, analyzed and discussed. The origins of the complex relation between TCO₃ and
125 SNO₂ in and around the Antarctic stratospheric vortex are briefly hypothesized and recommendations are provided about how satellite data of SNO₂ columns could be further explored and used for studying stratospheric nitrogen.

2. Satellite data sources and data selection

2.1 TROPOMI stratospheric NO₂ data

130 The Sentinel-5 Precursor (S5P) satellite, launched on 13 Oct. 2017 in an ascending sun-synchronous polar orbit, with an equator crossing at about 13:30 local time, carries the Tropospheric Monitoring Instrument (TROPOMI; Veefkind et al., 2012). This instrument provides measurements in four channels (UV, visible, NIR and SWIR) of several atmospheric trace gases (such as NO₂, O₃, SO₂, HCHO, CH₄, CO) and of cloud and aerosol properties.

135 The TROPOMI NO₂ data retrieval is performed from the visible band (400–496nm), with a spectral resolution and sampling of 0.54 nm and 0.20 nm, respectively, and a signal-to-noise ratio of around 1500. Individual ground pixels measure in the along-track direction 5.6 km (7.2 km prior to 6 Aug. 2019) and in the across-track direction 3.6 km at the middle of the swath, which increases to about 14 km near the edges of the swath. The full swath is about 2600 km wide, which means that TROPOMI achieves global coverage each day, except for narrow strips between orbits of about 0.5° wide at the equator.

140 The NO₂ retrieval process (van Geffen et al., 2022a, 2022b) uses the three-step approach introduced for OMI (Boersma et al., 2007, 2011). First a Differential Optical Absorption Spectroscopy (DOAS) is applied to determine the slant column density, the total amount of NO₂ along the effective light path from sun through atmosphere to satellite. A temperature correction is applied to correct for the temperature dependence of the NO₂ cross sections, based on collocated temperature profiles from ECMWF (re)analysis data. Then information on the NO₂ vertical profile shape taken from a chemistry transport model / data assimilation system (for TROPOMI: TM5-MP) that assimilates the slant columns is used to determine the
145 stratospheric vertical column density, symbolized hereafter by N_v^{strat} . The final step determines the tropospheric vertical column using appropriate air-mass factors (AMFs). The total vertical column density can be determined either from the sum of the two sub-columns or directly from the retrieved slant column – which of these total columns is the appropriate one depends on the application, as described in the Product User Manual (PUM; Eskes et al., 2022).

150 Since most of the NO₂ is located in the stratosphere, this study looks only at N_v^{strat} , the precision of which is estimated to be approximately 2×10^{14} molec.cm⁻² (3.3 μmol m⁻²) in the data assimilation. The spatiotemporal variations in SNO₂ are also seen in TNO₂ and the geometric NO₂ column (*i.e.* the slant column divided by the geometric AMF, *i.e.* without any model information; *cf.* van Geffen et al. (2022a)), but not in the tropospheric column. TROPOMI NO₂ data is reported in SI units, *i.e.* in mol m⁻², where the conversion factor to the more commonly used unit molecules cm⁻² is 6.022×10^{19} mol⁻¹.

155 The data used for this study comes from the version v2.3.1 intermediate S5P-PAL reprocessing (<https://data-portal.s5ppal.com/products/NO2.html>; last access: 06 Dec. 2022) over the period 1 May 2018 up to 14 Nov. 2021, followed by the operational v2.3.1 and v2.4.0 processing. The latter version change has little to no impact on the stratospheric NO₂ column and can therefore be ignored in this study. For some info on the different versions, see van Geffen et al. (2022a), the Product ReadMe File (PRF; Eskes et al., 2021) and the latest PRF of the operational product (Eskes and Eichmann, 2022).

The stratospheric NO₂ column of all ground pixels with valid retrieval (qa_value > 0.50) of all 14 or 15 orbits of a given day, *i.e.* orbit files with a start date & time in the file name for that day (irrespective of the actual sensing start and end), are arithmetically averaged on a 0.8° × 0.4° grid (*i.e.* there are in total 450 by 450 grid cells globally). A qu_value > 0.5 excludes any TROPOMI observation with a solar zenith angle > 81.2. During the Antarctic summer this leads to some observations from the descending TROPOMI orbit over Antarctic to be include in the daily average (TROPOMI orbits the sunlit part of the earth from south to north). No weighting in space, time, or with measurement errors is applied. The daily gridded data is more convenient for various statistical analyses than using daily orbit data, for example for spatiotemporal averaging. We will return in the discussion section 4 to the question whether the gridding and averaging matters for the results presented here.

2.2 TROPOMI stratospheric and/or total NO₂ column validation

It is well established that nadir viewing satellite measurements of TNO₂ are of good quality (Bortoli et al., 2013). An extensive first global validation of TROPOMI NO₂ can be found in Verhoelst et al. (2021). To highlight the quality of TROPOMI TNO₂ data over and around Antarctica we explore TROPOMI data collocated with ground-based stations from the SAOZ network. The data is conveniently provided and visualized at the TROPOMI validation facility and the TROPOMI validation server (<https://mpc-vdaf.tropomi.eu/> & <https://mpc-vdaf-server.tropomi.eu/>). Extensive evaluation and reports are provided at the validation facility and server and in quarterly validation reports (Lambert et al., 2023) where also details about the SAOZ data can be found. We selected five Southern Hemisphere surface stations for comparing SAOZ sunrise data with TROPOMI SNO₂ data from the TROPOMI offline data stream. These five stations are located inside and outside of the vortex and also sample the vortex edge (Table 1). To account for the often large difference in solar local time between the satellite (afternoon) and ground-based (twilight) observations, a diurnal cycle correction is applied based on model calculations. According to Compernolle et al. [2020] and Lambert et al. [2023] “the SAOZ measurements are adjusted to the TROPOMI overpass time using a model-based factor. This is calculated with the PSCBOX 1D stacked-box photochemical model (Errera and Fonteyn, 2001; Hendrick et al., 2004), initiated with daily fields from the SLIMCAT chemistry transport model (CTM). The uncertainty related to this adjustment is in the order of 10%. To reduce mismatch errors due to the significant horizontal smoothing differences between TROPOMI and SAOZ measurements, TROPOMI SNO₂ values (from ground pixels at high resolution) are averaged over the air mass footprint where ground-based zenith-sky measurements are sensitive”. The random error of SAOZ NO₂ total column measurements has been estimated at 4.7% with a total accuracy of 5.9% (Hendrick et al., 2011). See Verhoelst et al. (2021) as well as the TROPOMI validation server for more details.

Figure 1A shows a time series of the comparison of TROPOMI stratospheric NO₂ data with the SAOZ observations at the Antarctic site of Dumont d’Urville for the period 2018-2022. The Dumont d’Urville site is chosen as it is located sufficiently far north to provide good sampling of the seasonal stratospheric NO₂ cycle while also sampling both inner and outer Antarctic stratospheric vortex air during local spring. Note that observations are missing during the middle of winter at Dumont d’Urville due to the polar night. Figure 1B shows the scatter plot of the same data.

Overall, the satellite measurements and ground-based measurements at Dumont d'Urville agree well (Table 1). The correlation coefficient is 0.88 (R^2) with a bias of less than 2% and root means square differences of approximately 10%. The regression coefficient equals 0.94 and almost 1.0 dependent on the regression method. The measurements at Dumont
195 d'Urville during Antarctic springtime sample both inner and outer vortex air as evidenced by the rapid changes between large and small SNO₂ values during springtime. The validation results for Dumont d'Urville thus cover a wide range of atmospheric conditions. Results for the other four stations are rather similar (Table 1). Figures for the other four chosen validation sites can be found in the appendix (Figures A2A and A2B) as well as on the TROPOMI validation server. The validation results for all stations can be summarized as follows:

- correlations (R^2) are always better than 0.80 and up to 0.96
- biases are of the order of a few percent (11% for Rio Gallegos, Patagonia)
- root-mean-square differences vary between 10-20%
- standard errors are smaller than 1%
- 205 • regression values vary between 0.8 and 0.95
- results are fully consistent with Verhoelst et al. (2021)
- results are fully consistent with Lambert et al. (2023)

Note that for Rio Gallegos the bias is larger than for the other four locations used here (ground-based total NO₂ columns
210 larger than TROPOMI total NO₂ columns). One possible explanation could be that the SAOZ measurement location at Rio Gallegos is within 5 km from the edge of the buildup area of Rio Gallegos and 10 km from the city center. Lambert et al. [2023] found that for 42 polluted locations worldwide Pandora total NO₂ columns were on average approximately 18% larger than corresponding TROPOMI total NO₂ columns, not unlike the 11% bias for Rio Gallegos. For low pollution and clean locations the bias was smaller and reversed (TROPOMI total NO₂ columns approximately 6% larger than Pandora total
215 NO₂ columns. No large dependencies were found for the satellite solar zenith angle (SZA), the satellite cloud fraction and satellite surface albedo. Given that Rio Gallegos is a city of approximately 80,000 inhabitants and its proximity to the SAOZ measurement site it is not unlikely that Rio Gallegos SAOZ measurements could be contaminated by local air pollution under favorable wind conditions although it is beyond the scope of this paper to investigate this in detail. Note that given the large seasonal cycle in total NO₂ columns an 11% bias is still very well acceptable.

220 Given that the typical seasonal cycle and differences between inner and outer vortex air vary by a factor of two to five, standard errors are a few percent or less combined with very high correlation coefficients and regression coefficients are close to one, shows that single TROPOMI stratospheric NO₂ column measurements are of high quality and likely useful for in-depth exploration of spatiotemporal Antarctic stratospheric NO₂ variability.

2.3 Global ozone field data

225 In this study assimilated TROPOMI NO₂ column pixel data is used and gridded at a spatial resolution much coarser than
the original TROPOMI resolution while also averaging in time due to multiple polar overpasses per day as the main interest
in this first exploratory study is at phenomena at continental scales. However, the TROPOMI NO₂ column pixel data itself
are also already postprocessed level 2 observations, *i.e.* TROPOMI NO₂ data derived from a data assimilation system and in
that sense not pure level 2 pixel data anymore. Hence, it was decided to compare the TROPOMI NO₂ data with gridded
230 assimilated TCO₃ data rather than TCO₃ data at orbit level. An obvious TCO₃ dataset top use would be the Multi Sensor
Reanalysis version-2 (MSR-2; van der A et al., 2010, 2015) which provides a global reanalysis of TCO₃ combining multiple
and sometimes overlapping satellite measurements using an advanced ground-data-based approach to minimize inter-
satellite-instrument TCO₃ differences and biases. However, the MSR-2 TCO₃ dataset had not yet been extended in time to
cover the entire period for which TROPOMI NO₂ data was available. Hence the KNMI operational daily global assimilated
235 TCO₃ field is used here (Eskes et al., 2003; van der A et al., 2015; <https://www.temis.nl/protocols/O3global.php>, last access:
06 Dec. 2022) which is based on TCO₃ level 2 data products of the GOME-2 instruments aboard the MetOp satellites
(Munro et al., 2006, 2016). This operational TCO₃ field is produced by KNMI for operational UV index predictions up to
nine days ahead in time. GOME-2-based TCO₃ analyses are thus always available in real-time – unlike MSR-2 which is
currently updated only once per year. From this operational TCO₃ dataset the global total ozone field at each longitude at
240 local solar noon is used, which is close to the TROPOMI measurement time (section 2.1) and which is available for every
day of the year for the full globe. The local solar noon ozone field is, for example, used for the operational TEMIS UV index
and UV dose processing (van Geffen et al., 2017; Zempila et al., 2017). The local solar noon global TCO₃ field is given at a
longitude-latitude grid of 1.5°×1.0° and is re-gridded (bi-linear interpolation) to a finer 0.8°×0.4° to match the gridded NO₂
data. Note that differences between the KNMI operational daily global assimilated TCO₃ data and the MSR-2 TCO₃ data are
245 small. GOME-2 has a 4 DU offset relative to ground observations (MSR-2 has none) but otherwise GOME-2 and MSR-2
have similar root-mean square differences compared to ground observations (van der A et al., 2015). Hence, for the purpose
of this study both datasets would be interchangeable. The question of whether using assimilated TCO₃ data rather than
collocated TROPOMI TCO₃ orbit data will be discussed in section 4.

3 Data analysis and results

250 3.1 spatiotemporal variability

Figure 2 shows maps of the spatial distribution of SNO₂ and TCO₃ at local solar noon on 1 November 2018 as an
example of daily data. In both panels a black line displays the TCO₃ = 200 DU contour, a not uncommon reference value to
mark the edge of the Antarctic ozone hole for the Southern Hemisphere polar vortex.

SNO₂ depleted Antarctic inner vortex air and enhancement of SNO₂ around the edge of the polar vortex are clearly
255 visible. Figure 3 shows the same data as in Figure 2 but for an Antarctic polar view and with a different color scale. There
are clear similarities between the spatial patterns in SNO₂ and TCO₃. First of all, both show a significant reduction of values
within the Antarctic stratospheric vortex. Secondly, values for both are strongly enhanced equatorward just outside of the
vortex. Third, further equatorward of 45°S values of both start to decrease. And fourth: outside of the vortex values for both
are reduced around 0° longitude and enhanced at the opposite side towards 180° longitude (wave-1 pattern).

260 However, there are also clear differences. The SNO₂/TCO₃ ratio for example does not show a clear vortex edge (Noxon
cliff) like in both separate products. Furthermore, the gradient from the vortex edge towards the equator is smaller for TCO₃
than it is for SNO₂. These similarities and differences point to different processes governing their respective spatiotemporal
variations: chemistry (sources & sinks) and stratospheric dynamics (source and sink regions and transport from sources to
sinks).

265 Figure 4 shows the evolution of zonal averages of the SNO₂ during the four Southern Hemisphere summers from 2018
to 2021, with the 200 DU ozone contour indicated by a black line. From these figures it is clear that the springtime SNO₂
enhancement outside of the Antarctic vortex is kept out of the vortex during 2018, 2020 and 2021. The lack of such a well-
defined SNO₂ depleted area in 2019 is related to the weak Antarctic stratospheric vortex during spring 2019, which led to
weak ozone depletion (Safiedinne et al., 2020; Wargan et al., 2020; Stone et al., 2021) and according to the TROPOMI NO₂
270 data thus also led to less denitrification. This is consistent with results found for IASI HNO₃ (Wespes et al., 2022).

3.2 Correlating SNO₂ and TCO₃: 2D phase diagram

Figure 5 displays TROPOMI TCO₃ and SNO₂ data for 1 November 2018 as a 2D histogram (phase diagram; panel A)
revealing rather intricate patterns. For reasons explained below, the histogram was divided into three areas to be able to
discriminate between the inner-vortex, outer-vortex and the vortex edge. For the area “MASK 1” SNO₂ and TCO₃ show a
275 well-defined linear relationship. The area is associated with the inner vortex and is characterized by small TCO₃ values. The
area “MASK 2” represents air outside of the vortex characterized by larger TCO₃ values and somewhat larger SNO₂ values
than for the “MASK 1” area. Also, there is not such a well-defined linear relation between TCO₃ and SNO₂ for the “MASK
2” area as there is for the “MASK 1” area. The relation between TCO₃ and SNO₂ for “MASK 3” is much more intricate with
what appear to be “coherent line structures” connecting the “MASK 1” and “MASK 2” areas. These “mixing lines” – by lack
280 of better expression - are found for both small and large TCO₃ and SNO₂ values. The largest SNO₂ values are found in the
“MASK 1/3” areas whereas the largest TCO₃ values are found in the “MASK 2/3” areas. Note that the logarithmic color
scale enhances the focus on parts of the distribution that are less frequent. There are thus essentially two populations: inside
the vortex and outside the vortex. 16% of the histogram bins contain two thirds (~ 67%) of the data points and only
approximately 10% of the data qualifies for MASK-3.

285 3.3 multi-day periods and multi-annual data

Two key follow-up questions are whether these results change significantly over time. Figure 6 shows phase diagrams similar to the one displayed in Figure 5 but for days combined during multiple day intervals (5-10-15-30 days) starting at 1 November 2018. Although this means that each panel covers a different time period, the results are nevertheless very consistent. The distinction of two clear concentrated populations and the “mixing lines” is present for each time period. The results do also reveal a relation between TCO_3 and SNO_2 outside of the vortex albeit with a much larger spread. The high correlation between TCO_3 - SNO_2 inside the vortex is also present during all periods. The distribution does shift towards larger SNO_2 values due to increasing SNO_2 as part of the natural springtime SNO_2 cycle. Similarly – albeit more difficult to distinguish in Figure 6, outer vortex TCO_3 values become slightly smaller due to the natural seasonal springtime non-catalytic photochemical destruction of stratospheric O_3 . However, for inner-vortex air the TCO_3 distribution shifts towards larger TCO_3 values, reflecting the effects of dynamical mixing extra-vortex O_3 -rich (upper) stratospheric air during late spring (de Laat and van Weele, 2011).

Figure 7 shows similar panels as in Figures 5 and 6 but for 5-day periods starting at the first day of each month from September to December 2018. The results are much more variable than for the multi-day differences highlighting the strong seasonality of especially Antarctic stratospheric inner-vortex TCO_3 and SNO_2 . During early September O_3 depletion has yet to commence. There are already two separate populations discernible but TCO_3 values are still larger than 200 DU. SNO_2 values are generally small, especially within the Antarctic vortex due to the denitrification process. Early October 2018 the catalytic O_3 destruction has strongly reduced stratospheric O_3 . There is a group of datapoints with small TCO_3 values and small SNO_2 values. The air outside of the vortex is still characterized by large TCO_3 values and still relatively small SNO_2 values but larger values than during early September 2018. The “mixing lines” are also clearly discernible covering the entire phase space between both main populations. The picture for early November 2018 is rather similar albeit that SNO_2 values have further increased due to the natural seasonal cycle in SNO_2 . By early December 2018 the distribution is squeezed and values from both main populations are closer together. The vortex has largely disintegrated although remnants can still be discerned in TCO_3 but interestingly enough not in SNO_2 (see animation in the Supplementary Information). Remarkably the populations still cover the three previously defined areas “MASK1/2/3”. This indicates that $\text{TCO}_3/\text{SNO}_2$ ratios are rather useful for characterizing the origins and locations of stratospheric air masses.

Figure 8 displays similar results as in Figure 7 for early October but for all years from 2018 to 2021. The results for 2018, 2020 and 2021 are very similar providing further support for the notion that the $\text{TCO}_3/\text{SNO}_2$ ratios can be used to characterize the origins and locations of stratospheric air masses. The results for 2019 are quite different, reflecting the unusually weak 2019 Antarctic stratospheric vortex. There are still two populations in 2019 albeit only weakly separated. TCO_3 and SNO_2 values inside the vortex are larger compared to the other years. Overall, the anomalous 2019 vortex has a clear imprint on the TCO_3 and SNO_2 distributions. Note that during early September 2019 the amount of SNO_2 depletion was still similar to those in 2018-2020-2021 (not shown). The normal vortex pre-conditioning during Austral winter 2019

thus was not unusual which is consistent with published analyses of the 2019 Antarctic springtime vortex (Wargan et al., 2020; Smale et al., 2021; WMO, 2022). The faster 2019 increase in SNO₂ by early October compared to 2018-2020-2021 indicates that dynamics and mixing with - or influx of - NO₂-rich extra-vortex air is the main cause. Otherwise the SNO₂ increase would have been slower and more in line with the other three years.

3.4 Qualitative explanation of phase diagram results

The consistency of patterns in the spatiotemporal variations in the TCO₃-SNO₂ distributions suggest some very basic underlying processes. For example, differences in the location of the TCO₃ cross-vortex gradient relative to the location of the Noxon cliff for SNO₂ should show up as patterns in the phase diagram. To provide a qualitative explanation of the observed patterns two simple series of longitudinal and latitudinal variations in TCO₃ and SNO₂ were created. For the first one, TCO₃ and SNO₂ vary as a sine wave along longitudes but with a different longitudinal phase (Figure 9). For the second one, TCO₃ and SNO₂ increased from pole to middle-latitudes and then decrease toward the equator to resemble the Noxon cliff but with a slightly different latitudinal change visually mimicking the observed TCO₃ and SNO₂ latitudinal gradients. Figure 9 shows the results for the relation between both. For the phase-shifted sine wave functions, the results obviously show up as an oval. The latitudinal shifted results however follow a curve qualitatively not dissimilar from the observed “mixing lines”. These results thus support the observation that the cross-vortex TCO₃ gradient and SNO₂ Noxon cliffs do not occur at the same locations which results in the emergence of “mixing lines” in the phase diagrams.

4 Discussion

The results presented here show that TROPOMI provides high quality daily SNO₂ data for monitoring variations in SNO₂ both inside and outside the Antarctic stratospheric vortex. It allows for studying the “nitrogen hole” - the denitrification process, as well as the “Noxon cliff” – the sharp gradient in trace gas amounts along the vortex edge, and associated seasonal changes during Antarctic springtime and interannual variability. Furthermore, combining the SNO₂ data with high quality TCO₃ data in phase diagrams reveals coherent patterns – “mixing lines” - linking the Antarctic stratospheric air inside and outside the vortex.

A clear discrepancy was found between the location of the SNO₂ Noxon Cliff and the TCO₃ cross vortex gradient. The few studies that provide information on the joint vertical distributions of NO₂ and O₃ suggest that the bulk of stratospheric NO₂ is found at higher altitudes than the bulk of stratospheric O₃ (Ridley et al., 1984; Lindenmaier et al., 2011). Differences in bulk heights which mostly determine total column variability link to differences in advection processes and might explain differences in the location of the NO₂ Noxon cliff and the cross-vortex TCO₃ gradient. Explorative studies using stratospheric chemistry models likely should help unraveling these issues. This in turn may contribute to developing applications and metrics for stratospheric NO₂-column-based Antarctic ozone hole monitoring. In addition, the notion of different bulk heights is consistent with the notion that the break-up dates or final warming of the Antarctic stratospheric

vortex occurs later for lower stratospheric altitudes (higher pressure levels) (Butler et al., 2021; Lecouffe et al., 2022). For
350 example, by late November 2018 there still is well defined area with reduced TCO_3 for which reduced SNO_2 has already
vanished (see animation in the Supplementary Information). A lower bulk height for TCO_3 compared to SNO_2 would mean
that SNO_2 anomalies would vanish earlier, as observed.

Furthermore, a strong inner-vortex correlation between SNO_2 and TCO_3 was found which was absent outside of the
vortex. The SNO_2 - TCO_3 phase diagrams display a clear dynamical cycle reflecting springtime changes in chemistry and
355 dynamics. This cycle was consistently seen in multiple years (2018-2020-2021) but was significantly different in 2019, a
year with a strongly perturbed Antarctic springtime vortex. Qualitatively the coherent patterns in the phase diagrams can be
explained by spatiotemporal differences in the phases of SNO_2 and TCO_3 , *i.e.* where and when minima and maxima occur in
 SNO_2 and TCO_3 . SNO_2 and TCO_3 are clearly not always and not everywhere *in sync*. This in part appears to be associated
with the differences in Antarctic stratospheric denitrification and O_3 depletion. Denitrification is a wintertime process
360 starting already by early winter and causing the Antarctic stratosphere to be significantly depleted of nitrogen by the time
sunlight returns (and thus TROPOMI starts to provide inner-vortex observations). The O_3 destruction cycle on the other hand
critically depends on the presence of sunlight. At the start of springtime O_3 depletion has yet to speed up. During the month
of September the amount of sunshine and duration of sunshine rapidly increase causing a rapid deepening of the Antarctic
Ozone Hole. Hence, the denitrification and O_3 depletion cycles differ significantly in their timing. Similarly, the results also
365 revealed an earlier disappearance of the “ NO_2 hole” relative the “Ozone hole”, further supporting the notion that differences
in chemistry and dynamics govern the differences in SNO_2 and TCO_3 behavior.

The observation of coherent spatial line structures (“mixing lines”) in relation to stratospheric transport and mixing –
including stratosphere-troposphere exchange - is not new. The presence of layered trace gas structures in the stratosphere
(laminae, filamentation, contour advection (Waugh and Plumb, 1994; Newman et al., 1996; Appenzeller and Holton, 1997;
370 Orsolini and Grant, 2000; Who and Lagras, 2002)) is closely associated with the stability of the stratosphere, the
conservation of potential vorticity and isentropic mixing (Waugh and Polvani, 2010). Stratospheric air masses often organize
themselves in such long-lived laminae. For example, satellite observations of direct injection of volcanic material directly
into the (lower) stratosphere have provided many examples of laminae development and filamentation because of the ability
of satellites to observe sulfur dioxide and volcanic ash (Krotkov et al., 2021; de Leeuw et al., 2021; Kahykin et al., 2022).
375 Satellite observations of aerosols from wildfires have started to be used for similar purposes for stratospheric smoke
(Khaykin et al., 2020; Magaritz-Ronen and Raveh-Rubin, 2021). And complex relationships among (long-lived)
stratospheric trace gases have been used for understanding stratospheric dynamics (*e.g.* Hoor et al., 2002; Plumb, 2007;
Barre et al., 2012; Hoffmann et al., 2017; Krasauskas et al., 2021). How exactly these processes and concepts relate to the
observed “mixing lines” would make a relevant topic of future research.

380 Furthermore, model simulations could be used to assess (1) whether model simulations show similar phase diagrams and
if so, (2) whether the model simulations contain clues for explaining the differences in spatiotemporal SNO_2 and TCO_3
behavior. The model simulations might also reveal caveats and missing processes in the model representation of

stratospheric chemistry and Antarctic stratospheric vortex dynamics. In addition, the results can also be further explored towards a more thorough conceptual explanation of SNO₂ variability. Comparison with IASI HNO₃ total columns might help
385 there as well, just like a comparison and evaluation of SNO₂ with satellite NO₂ profile measurements from for example the OSIRIS, ACE-FTS or MAESTRO satellite instruments. A comparison with IASI HNO₃ could for example be used to explore whether both are more *in sync* than SNO₂ is with TCO₃. Comparison with limb satellite NO₂ profile measurements in conjunction with O₃ profile measurements should provide indications of which altitudes mostly determine column observations of NO₂ and O₃. In addition, evaluation of results from a different dynamical framework of the equivalent
390 latitude might help improve understanding of Antarctic stratospheric vortex edge dynamics. This links to the important question of where and when vortex mixing takes place. It is well established that the Antarctic stratospheric vortex can be destabilized by increased extra-vortex wave activity. Direct observations of where and when that takes place is unclear but the combination of SNO₂ and TCO₃ (possibly extended with IASI HNO₃) might help identifying mixing regions.

An additional question is whether satellites other than TROPOMI that also measure SNO₂ might help extend the SNO₂
395 southern hemisphere record further back in time. A dataset going back to 2003 already exists via the QA4ACV NO₂ data (Boersma et al., 2018). The combination of GOME (1995-2011), SCIAMACHY (2002-2012), OMI (2003-now), GOME-2 (2007-now), and OMPS (2012-now) potentially allows for reconstructing an almost 30-year record of Southern Hemisphere mid-latitude and Antarctic SNO₂. Such a record could be probed for finding hints and clues of (Antarctic) stratospheric ozone recovery, as TCO₃ is expected to change much faster due to decreasing O₃ depleting substances than SNO₂ - mostly
400 due to emissions of N₂O and slowly increasing atmospheric N₂O concentrations (Struthers et al., 2004). Other processes relevant for Antarctic stratospheric NO₂ and O₃ are production of (upper) stratospheric NO_x by energetic electron precipitation and by increased downwelling of upper stratospheric air by the expected speeding up of the Brewer-Dobson circulation (Gordon et al., 2020; Maliniemi et al., 2021; Müller, 2021).

Furthermore, there are some other aspects for further exploration. The validation could be extended to more ground-
405 based comparison and more detailed evaluations. It could be assessed whether it matters if TNO₂ is used (based on data assimilation) rather than SNO₂. The assimilation SNO₂ data is important for deriving tropospheric NO₂ but not necessarily the best estimate of TNO₂. Note that there is no reason to assume that SNO₂ and/or TCO₃ data quality issues will change the findings of this paper, but only in-depth analyses will provide support for that assumption. In addition, although the diurnal cycle in SNO₂ is relatively small compared to its seasonal cycle it nevertheless can affect satellite retrievals and validation
410 results. Dubé et al. [2021] reported order of magnitude 10-20% diurnal cycle effects for SAGE III/ISS solar occultation limb retrievals with the largest effects found at higher latitudes. Although their results are not one-on-one applicable to the results presented here they clearly indicate the need for properly assessing diurnal cycle effects on TROPOMI SNO₂ measurements and validation.

In this study gridded SNO₂ was used to allow easy comparison with other data as Sentinel-5p data quality is still
415 improving and reprocessing of data is ongoing. A key question is whether results would differ for a Sentinel-5p pixel-level comparison of SNO₂ and TCO₃. A first brief assessment of using Sentinel-5p pixel-level comparison of SNO₂ and TCO₃ (see

appendix Figure A3) yielded very similar results, indicating that results presented here are robust relative to using gridded data or pixel data or even data from different satellites.

420 Finally, limited use of nadir-viewing satellite measurements of NO₂ for studying the Noxon Cliff and the Antarctic stratospheric denitrification process is somewhat surprising. The potential for their use to explore polar stratospheric chemistry and dynamics is evident from Wenig et al. (2004), Richter et al. (2005) and Adams et al. (2013). Satellite measurements of NO₂ - and tropospheric NO₂ column measurements - have been widely used for approximately two decades now. Total stratospheric NO₂ columns play an important role in deriving tropospheric NO₂ columns, as the stratospheric part needs to be removed from the total part (Boersma et al., 2003; Boersma et al., 2007; Boersma et al., 2018). This is typically
425 done by assimilating the satellite measurements of total NO₂ over clean regions into a numerical chemistry transport model to reconstruct the stratospheric column globally (Eskes et al., 2003; Boersma et al., 2004; Boersma et al., 2007). The assimilation therefore allows to determine the stratospheric column over polluted regions with sufficient accuracy and precision to subtract it from the total column to arrive at an accurate tropospheric column. This approach requires also sufficiently accurate measurements of stratospheric NO₂. Hence the quality of stratospheric NO₂ has for a long time been
430 assessed for various satellites (*e.g.* Boersma et al., 2004; Dirksen et al., 2011; Valks et al., 2011; Verhoelst et al., 2021; Lambert et al., 2023). Nevertheless, despite the fact that nadir stratospheric NO₂ column TROPOMI measurements turn out to be of very good quality their intrinsic value for stratospheric research has remained largely unrecognized.

5. Conclusions

This paper presents a first assessment of the use of Sentinel-5p SNO₂ measurements for studying Southern Hemisphere
435 middle latitude and Antarctic stratospheric processes including the Antarctic Ozone Hole.

Comparison of gridded SNO₂ and assimilated TCO₃ via phase diagrams reveals intricate patterns. Three different regimes could be clearly identified: the inner vortex, the vortex edge and the extra-vortex region. Each regime is associated with its own SNO₂/TCO₃ characteristics. The vortex edge was characterized by so-called “mixing lines” in SNO₂-TCO₃ phase diagrams. A certain misalignment of the SNO₂ Noxon cliff and cross-vortex TCO₃ gradient was found along the
440 Antarctic stratospheric vortex pointing to vortex-edge dynamics as the root cause. A possible explanation could be differences in bulk heights of SNO₂ and TCO₃ so that their respective total columns reflect processes occurring at different heights.

Springtime SNO₂-TCO₃ variations/changes are robust throughout single-day to multi-day statistics. Throughout spring the SNO₂-TCO₃ distributions change significantly as a result of chemistry and vortex dynamics including mixing of air inside and outside the vortex. Regarding interannual variability the distributions are very similar for 2018-2020-2021 but
445 significantly different from 2019 which was a year with an anomalously weak Antarctic stratospheric vortex and only weak O₃ depletion.

Seasonal changes in the phase diagrams indicate that both total column data products are sensitive to different heights and thus different processes. In general the vortex remains longer visible in TCO₃ data than in SNO₂ data. SNO₂ is less sensitive to the lower stratosphere— where the stratospheric vortex remains intact longer - than SNO₂ so the nitrogen hole

450 will disappear earlier than the ozone hole. Vertical tilting of the vortex edge combined with different vertical sensitivities likewise explains the presence of the third regime that in the phase diagrams linking the inner vortex regime with the outer vortex regime.

This study only presents a first glimpse of the great potential of high quality spatiotemporal satellite SNO₂ measurements for studying stratospheric chemistry and stratospheric dynamics as well as long term changes in stratospheric composition extending the SNO₂ record back in time in combination with for example the MSR-2 total ozone reanalysis (van der A et al., 2015). The ability to monitor stratospheric nitrogen is also more than welcome given that an important piece of stratospheric observational remote sensing capacity by way of the Microwave Limb Sounder (MLS) will end by 2025 or at the latest 2026 and no satellite missions are planned to fill the gap created by the end of the MLS mission.

460 *Author contributions.* A.d.L. wrote the paper and did the majority of data analysis and interpretation. J.v.G. did the data processing and participated also in the data analysis. P.S. is the instigator of this piece of research, J.P.V. is the PI of Sentinel-5p/TROPOMI, H.E. is responsible for the TNO₂ data assimilation product and R.v.d.A. maintains the TCO₃ data assimilation and data dissemination. All authors contributed to the discussion and interpretation of results.

465 *Competing interests.* The authors declare that they have no conflicts of interest.

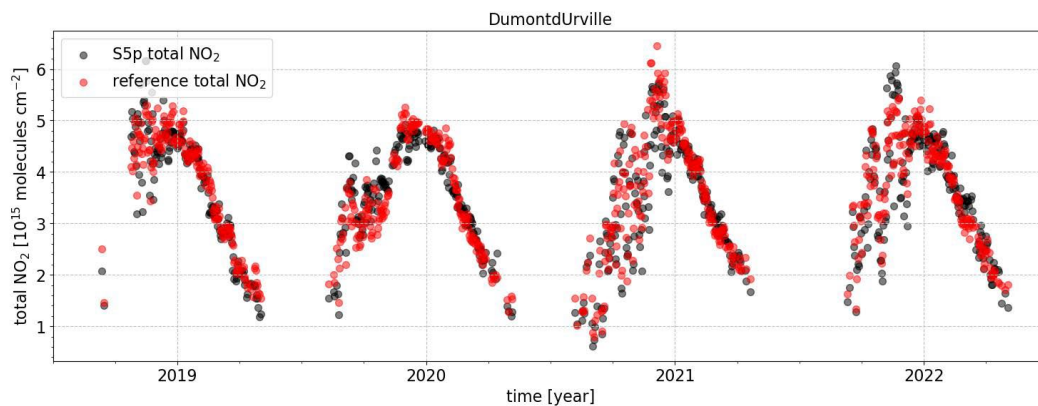
Data availability. Data used in this paper is available via the ESA Sentinel-5p hub (SNO₂), the TEMIS web portal (TCO₃) and the TROPOMI validation data facility (SAOZ data and collocated TROPOMI TNO₂ and TROPOMI assimilated SNO₂)

<https://s5phub.copernicus.eu/dhus/#/home>

470 <http://www.temis.nl>

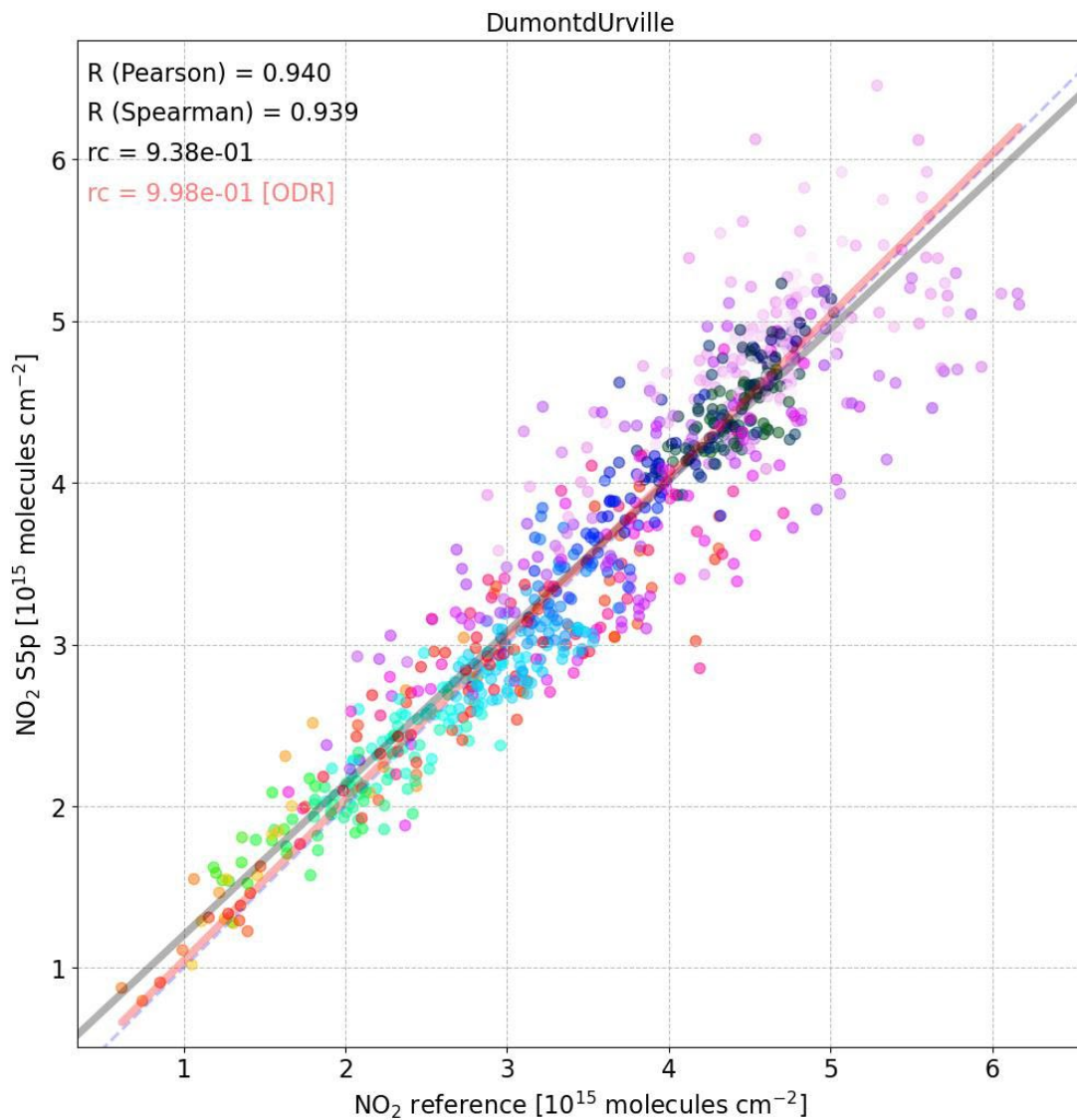
<http://mpc-vdaf.tropomi.eu/index.php/nitrogen-dioxide/>

Acknowledgements. Sentinel-5 Precursor is a European Space Agency (ESA) mission on behalf of the European Commission (EC). The TROPOMI payload is a joint development by ESA and the Netherlands Space Office (NSO). The Sentinel-5 Precursor ground-segment development has been funded by ESA and with national contributions from The Netherlands, Germany, and Belgium. This work contains modified Copernicus Sentinel-5P TROPOMI data (2018-2022), processed in the operational framework or locally at KNMI.

**Figure 1A.**

Comparison of S5p TNO₂ and SAOZ sunrise TNO₂ for the location of Dumont d'Urville. Data was directly obtained from
485 the Sentinel-5p validation facility where also more details can be found about the SAOZ data as well as similar data
visualizations (<http://mpc-vdaf.tropomi.eu/index.php/nitrogen-dioxide/> accessed 21 November 2022). Data markers are
semi-transparent to allow for visually discriminating between overlapping SAOZ and TROPOMI data points. Note that for

each SAOZ data point there is a corresponding TROPOMI data point.



490 **Figure 1B.**

Scatterplot of TROPOMI total NO₂ and SAOZ sunrise NO₂ as presented in Figure 1A. Regression coefficients are for an ordinary linear regression (OLR; grey line) and the orthogonal distance regression (ODR; red line) with 1:1 line shown by the grey dashed line. Colors represent different times of the year (see appendix Figure A1 for the corresponding colored version of Figure 1A).

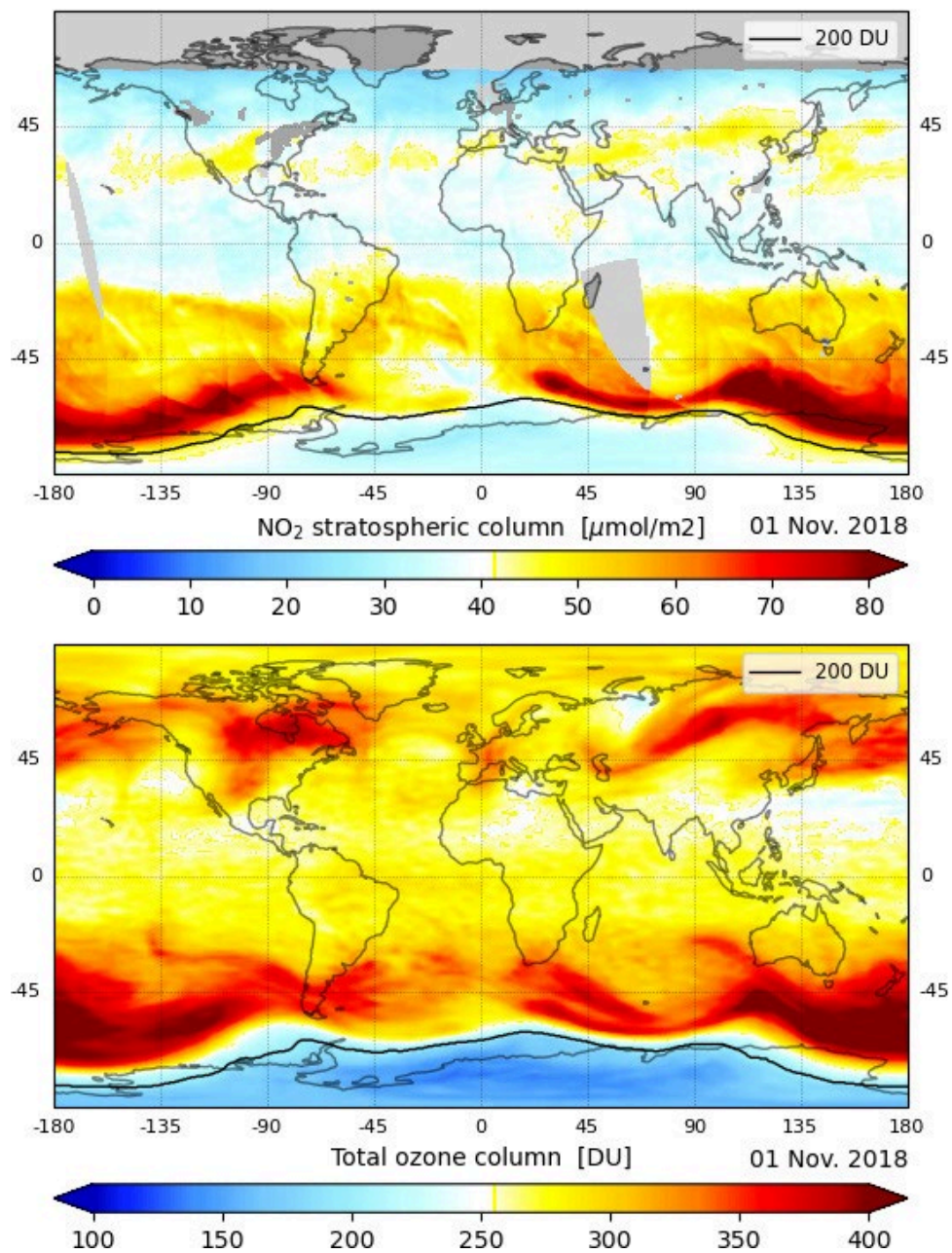


Figure 2.

Maps of globally gridded TROPOMI-based stratospheric NO₂ (top; in $\mu\text{mol m}^{-2}$) and globally gridded local solar noon
500 assimilated TCO₃ (bottom; in Dobson Units or DU) on 1 November 2018. The location of the 200 DU ozone contour is
indicated by a black line in both panels. Greys denote areas without TROPOMI data.

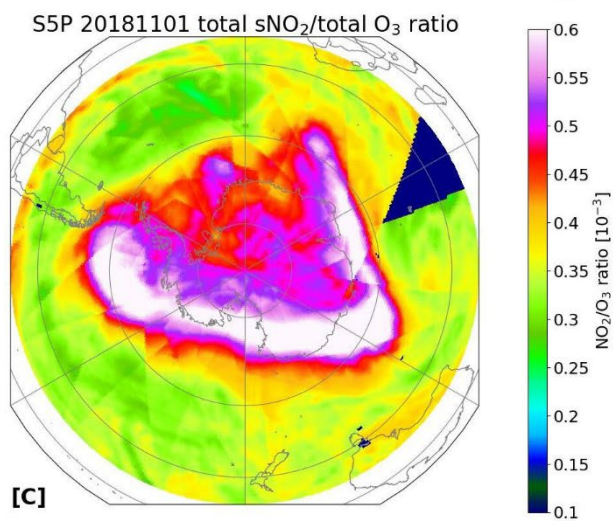
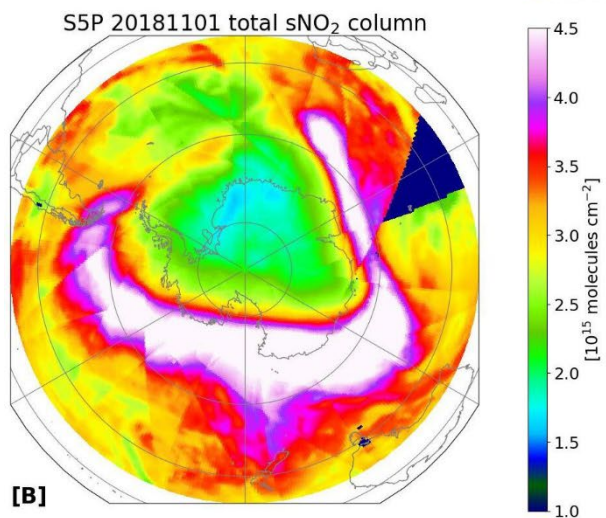
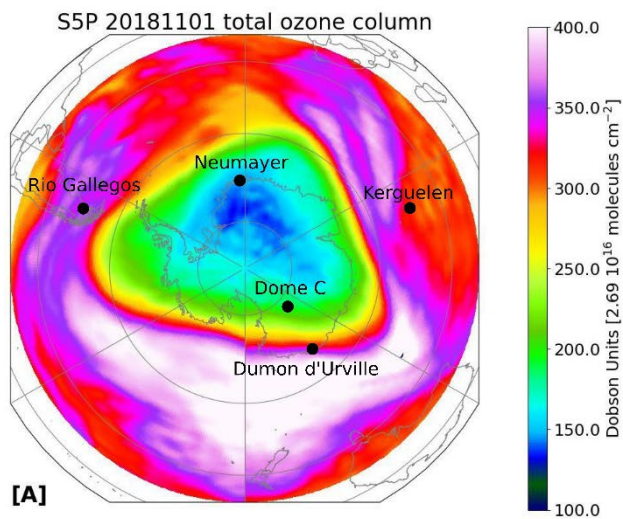


Figure 3.

505 As figure 2 (1 November 2018) but from an Antarctic polar view and with a different color scale. Panel C shows the $\text{SNO}_2/\text{TCO}_3$ ratio of panels A+B.

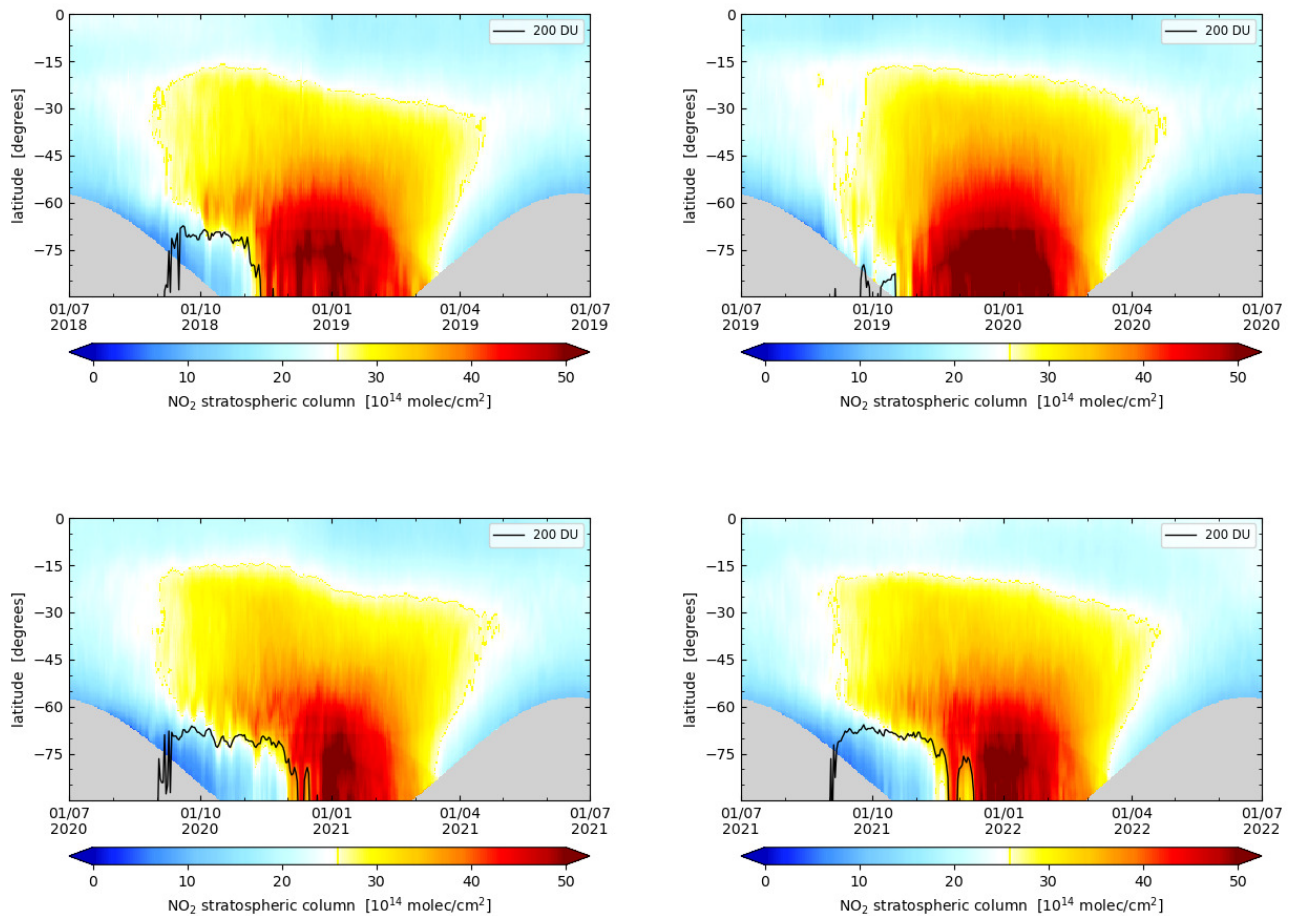
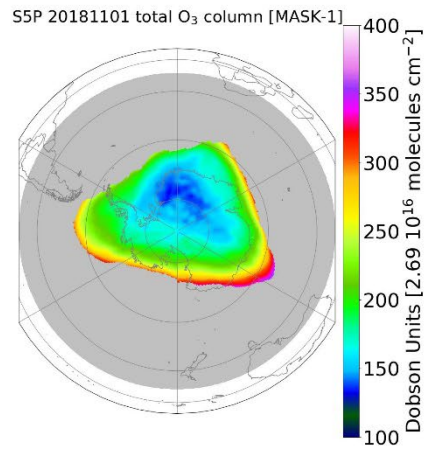
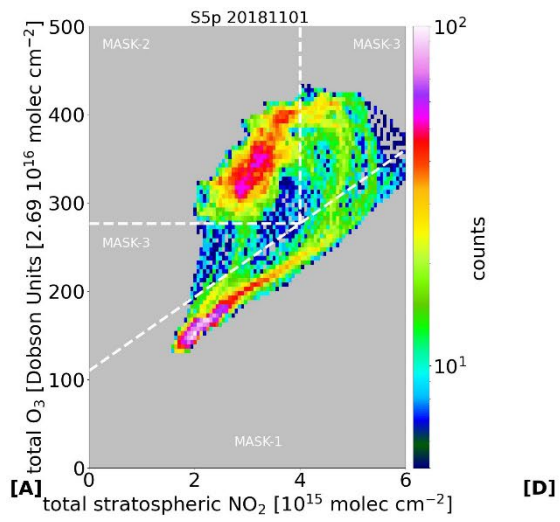
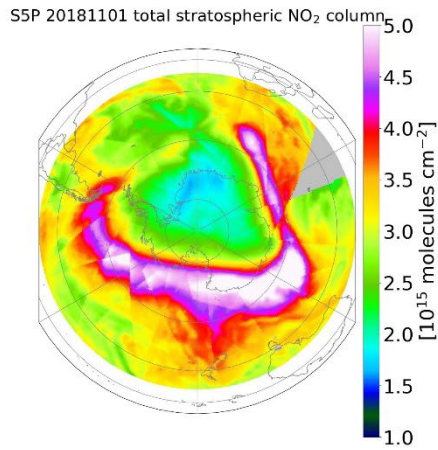


Figure 4.

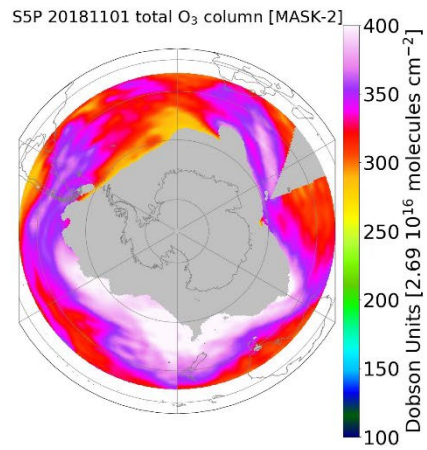
Maps of the Southern Hemisphere daily zonal average SNO_2 for four Southern Hemisphere summers (July-July) from 2018 to 2022. The location of the 200 DU ozone contour is indicated by a black line in all panels. Greys denote areas and times within TROPOMI data.



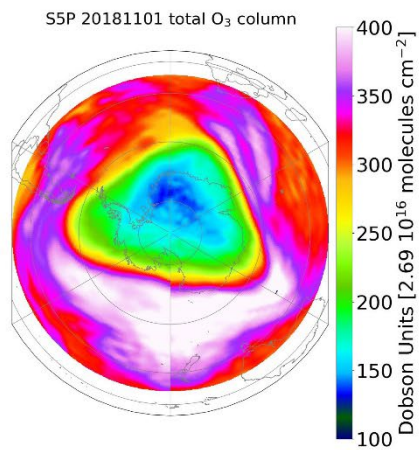
[D]



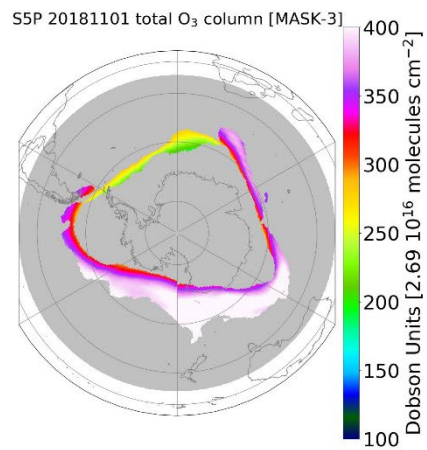
[B]



[E]



[C]



[F]

510 **Figure 5.**

[A] 2D histogram (phase diagram) of TROPOMI SNO₂ vs assimilated TCO₃ for 1 November 2018 and corresponding spatial distribution of SNO₂ (panel B) and TCO₃ (panel C) as in Figure 3. The phase diagram is color coded according to the logarithm of the number of counts. The phase diagram is a 100×100 pixel grid ranging between 0.0 - 6.0 10¹⁵ molecules cm⁻² SNO₂ and 0 - 500 DU TCO₃. [D], [E], [F]: spatial distribution of TCO₃ as in the lowest plot of the left column but filtered on the masking in the phase diagram in the upper left plot (D = MASK-1; E = MASK-2; F = MASK-3).

515

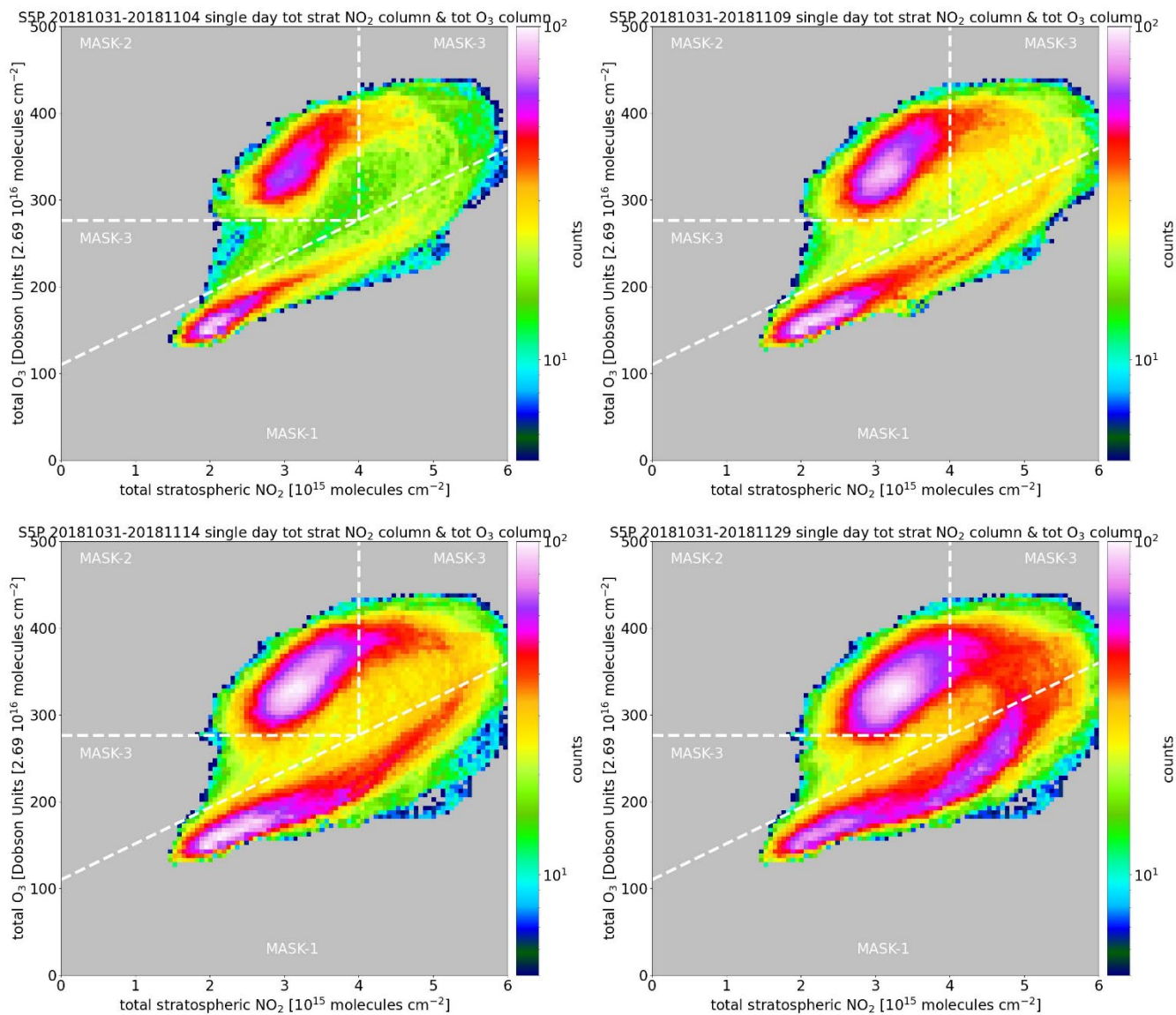


Figure 6.

Phase diagrams of TROPOMI SNO₂ and assimilated GOME-2 TCO₃ Similar to the phase diagram in Figure 5 (panel [A])

520 but for daily gridded data combining either 5, 10, 15 or 30 days starting at 31 October 2018.

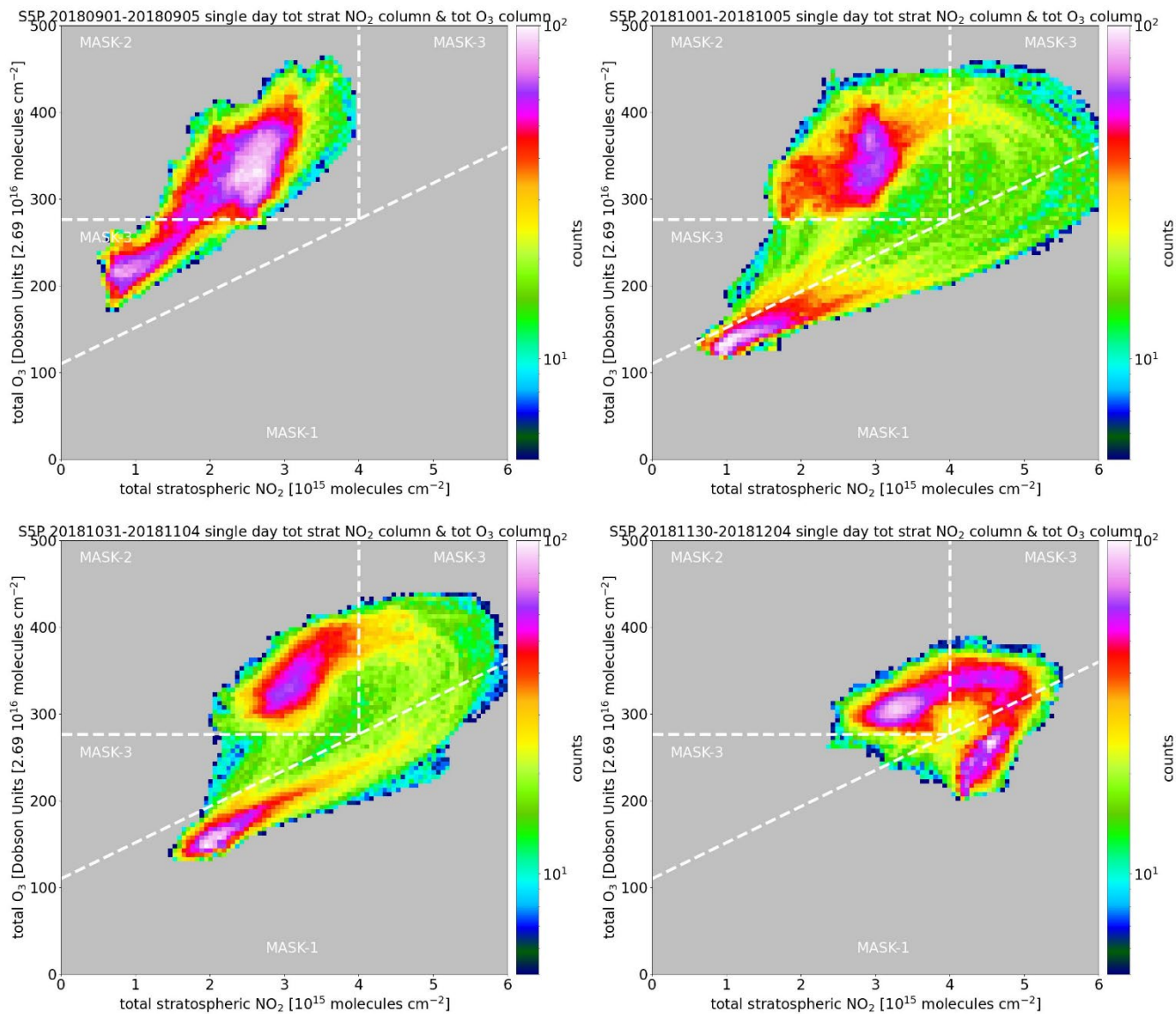
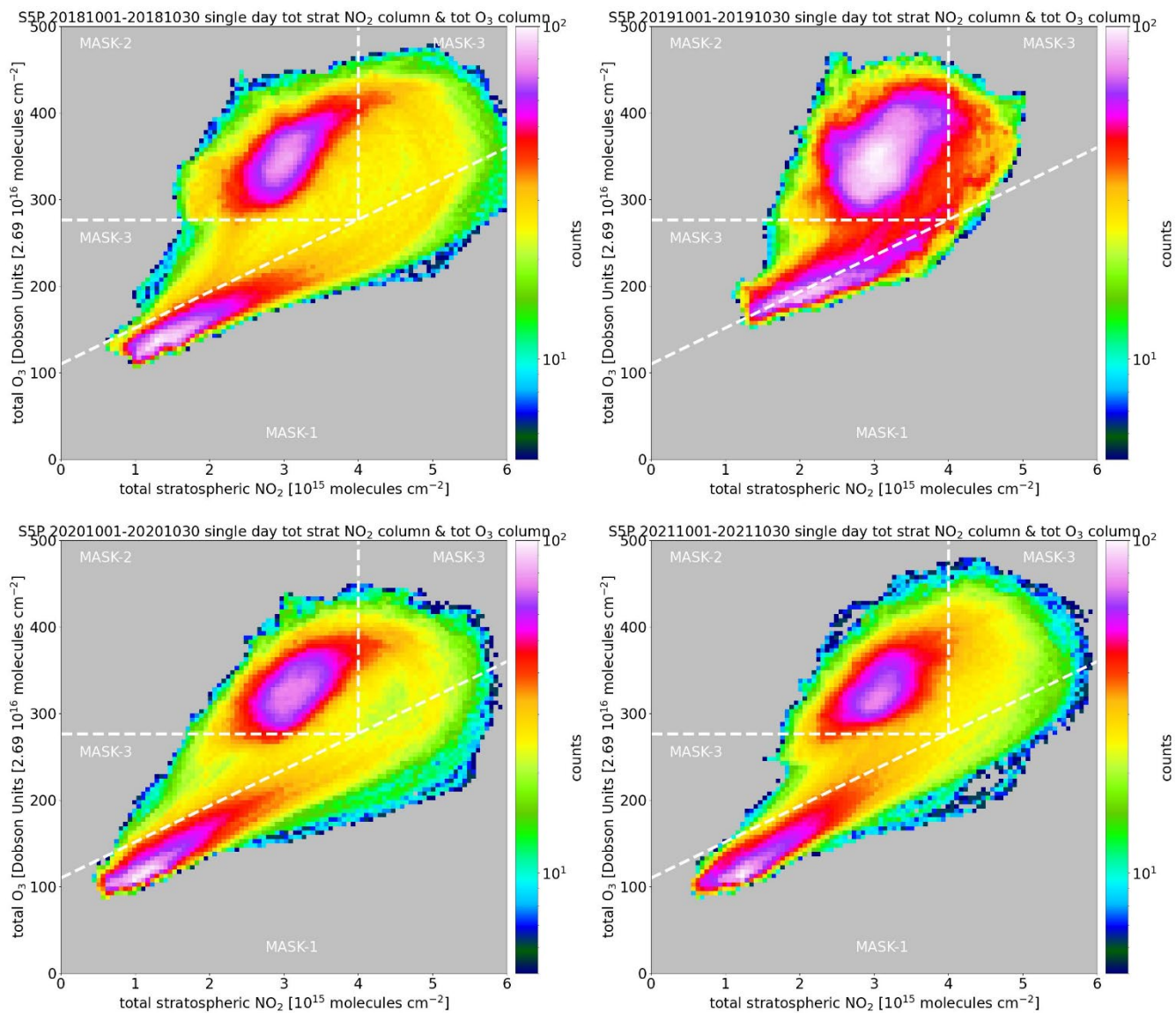


Figure 7.

As Figure 6 but for 5-day periods starting at 1 September, 1 October, 31 October and 30 November 2018.



525 **Figure 8.**

As Figure 6 but for 1-30 October of each year between 2018-2021.

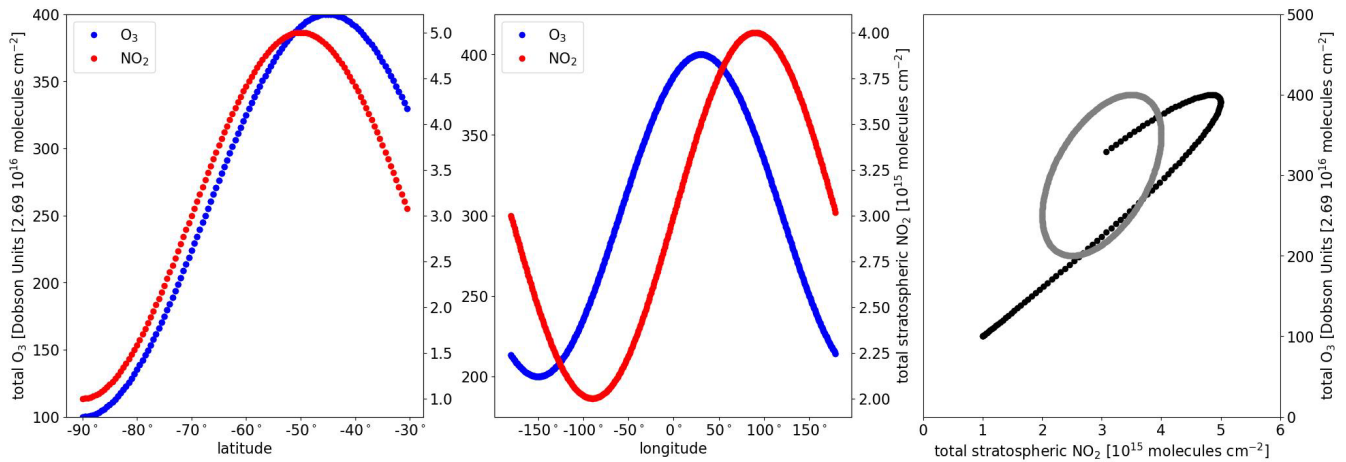


Figure 9.

Left panel: latitudinal SNO₂ and TCO₃ variations between 30S and 90S. The functions for SNO₂ and TCO₃ are slightly
 530 shifted in the latitudinal direction, with SNO₂ peaking earlier and decreasing faster towards the equator after the peak. The
 result of these two functions is indicated by the black line in the right panel. Right panel: longitudinal data and phase
 diagram of a data series (sine wave) for SNO₂ (red) and TCO₃ (blue) with a longitudinal phase shift of 90 degrees. The
 amplitude of the sine wave is chosen to represent observed values but otherwise just a scaling factor. The result for these two
 functions is indicated by the grey line in the right panel.

535

Tables

	R²	Bias 10¹⁵	Bias %	RMS 10¹⁵	RMS %	Fit
	[P]	[mean]	[mean]	(err)	(err)	[OLR]
	[S]	[median]	[median]			[ODR]
Kerguelen (49.35°S / 70.26°E)	0.906 0.914	-0.038 -0.065	-2.51 -2.54	0.291 (0.009)	10.23 (0.31)	0.786 0.818
Rio Gallegos (51.60°S / 69.32°W)	0.925 0.925	-0.282 -0.295	-11.39 -11.62	0.244 (0.007)	9.80 (0.27)	0.899 0.944
Dumont d'Urville (66.67°S / 140.02°E)	0.884 0.882	-0.039 -0.056	-0.88 -1.67	0.371 (0.013)	10.48 (0.36)	0.938 0.999
Neumayer (70.65°S / 8.24°W)	0.962 0.960	0.091 0.091	4.64 4.23	0.240 (0.012)	14.01 (0.72)	0.910 0.926
Concorde Dome (75.1°S, 123.35°E)	0.834 0.821	-0.035 -0.130	-2.36 -3.64	0.466 (0.023)	18.75 (0.93)	0.808 0.875

Table 1.

540 Comparison of southern hemisphere and Antarctic SAOZ sunrise measurements of SNO₂ (TNO₂) with TROPOMI SNO₂ observations. Correlations display the Pearson coefficient (P) and the Spearman coefficient (S). Fit coefficients are provided for the ordinary linear regression (OLR; top value) and the orthogonal distance regression (ODR; bottom balue).

References

- 545 van der A, R.J., Allaart, M.A.F., and Eskes, H.J. (2010): Multi sensor reanalysis of total ozone, *Atmos. Chem. Phys.*, 10, 11277–11294, <https://doi.org/10.5194/acp-10-11277-2010>
- van der A, R.J., Allaart, M.A.F., and Eskes, H.J. (2015): Extended and refined multi sensor reanalysis of total ozone for the period 1970–2012, *Atmos. Meas. Tech.*, 8, 3021–3035, <https://doi.org/10.5194/amt-8-3021-2015>
- Adams, C., Strong, K., Zhao, X., Bourassa, A.E., Daffer, W.H., Degenstein, D., Drummond, J.R., Farahani, E.E., Fraser, A.,
550 Lloyd, N.D., Manney, G.L., McLinden, C.A., Rex, M., Roth, C., Strahan, S.E., Walker, K.A., and Wohltmann, I. (2013): The spring 2011 final stratospheric warming above Eureka: anomalous dynamics and chemistry, *Atmos. Chem. Phys.*, 13, 611–624, <https://doi.org/10.5194/acp-13-611-2013>
- Appenzeller, C., and Holton, J.R. (1997): Tracer lamination in the stratosphere: A global climatology, *J. Geophys. Res.*, 102(D12), 13555–13569, <https://doi.org/10.1029/97JD0006>
- 555 Barbero, A., Savarino, J., Grilli, R., Blouzon, C., Picard, G., Frey, M.M., Huang, Y., and Caillon, N. (2021): New estimation of the NO_x snow-source on the Antarctic Plateau, *Journal of Geophysical Research: Atmospheres*, 126, e2021JD035062, <https://doi.org/10.1029/2021JD035062>
- Barré, J., Peuch, V.-H., Attié, J.-L., El Amraoui, L., Lahoz, W. A., Josse, B., Claeysman, M., and Nédélec, P. (2012): Stratosphere-troposphere ozone exchange from high resolution MLS ozone analyses, *Atmos. Chem. Phys.*, 12, 6129–6144,
560 <https://doi.org/10.5194/acp-12-6129-2012>.
- Beirle, S., Hörmann, C., Jöckel, P., Liu, S., Penning de Vries, M., Pozzer, A., Sihler, H., Valks, P., and Wagner, T. (2016): The STRatospheric Estimation Algorithm from Mainz (STREAM): estimating stratospheric NO₂ from nadir-viewing satellites by weighted convolution, *Atmos. Meas. Tech.*, 9, 2753–2779, <https://doi.org/10.5194/amt-9-2753-2016>
- Belmonte Rivas, M., Veefkind, P., Boersma, F., Levelt, P., Eskes, H., and Gille, J. (2014): Intercomparison of daytime
565 stratospheric NO₂ satellite retrievals and model simulations, *Atmos. Meas. Tech.*, 7, 2203–2225, <https://doi.org/10.5194/amt-7-2203-2014>
- Bodeker, G.E., Struthers, H., and Connor, B.J. (2002): Dynamical containment of Antarctic ozone depletion, *Geophys. Res. Lett.*, 29 (7), <https://doi.org/10.1029/2001GL014206>.
- Boersma, K.F., Eskes, H.J., and Brinksma, E.J. (2004): Error analysis for tropospheric NO₂ retrieval from space, *J. Geophys. Res.*, 109, D04311, doi:10.1029/2003JD003962.
570
- Boersma, K.F., Eskes, H.J., Veefkind, J.P., Brinksma, E.J., Van der A, R.J., Sneep, M., Van den Oord, G.H.J., Levelt, P.F., Stammes, P., Gleason J.F., and Bucsela, E.J. (2007): Near-real time retrieval of tropospheric NO₂ from OMI, *Atmos. Chem. Phys.*, 7, 2103–2128, <https://doi.org/10.5194/acp-7-2103-2007>
- Boersma, K.F., Eskes, H.J., Dirksen, R.J., Van der A, R.J., Veefkind, J.P., Stammes, P., Huijnen, V., Kleipool, Q. L., Sneep,
575 M., Claas, J., Leitão, J., Richter, A., Zhou, Y. and Brunner, D. (2011): An improved retrieval of tropospheric NO₂ columns from the Ozone Monitoring Instrument, *Atmos. Meas. Tech.*, 4, 1905–1928, <https://doi.org/10.5194/amt-4-1905-2011>

- Boersma, K.F., Eskes, H.J., Richter, A., De Smedt, I., Lorente, A., Beirle, S., van Geffen, J.H.G.M., Zara, M., Peters, E., Van Roozendael, M., Wagner, T., Maasakkers, J.D., van der A, R.J., Nightingale, J., De Rudder, A., Irie, H., Pinardi, G., Lambert, J.-C., and Compernelle, S.C. (2018): Improving algorithms and uncertainty estimates for satellite NO₂ retrievals: results from the quality assurance for the essential climate variables (QA4ECV) project, *Atmos. Meas. Tech.*, 11, 6651–6678, <https://doi.org/10.5194/amt-11-6651-2018>
- 580
- Bortoli, D., Ravegnani, F., Giovanelli, G., Kulkarni, P.S., Anton, M., Costa, M.J., and Silva, A.M. (2013)). Fifteen years of stratospheric nitrogen dioxide and ozone measurements in Antarctica. In *AIP Conference Proceedings* (Vol. 1531, No. 1, pp. 300-303). American Institute of Physics.
- 585
- Bortoli, D., Giovanelli, G., Ravegnani, F., Kostadinov, I., and Petritoli, A. (2005): Stratospheric nitrogen dioxide in the Antarctic, *International Journal of Remote Sensing*, 26:16, 3395-3412, <https://doi.org/10.1080/01431160500076418>
- Bourassa, A.E., McLinden, C.A., Sioris, C.E., Brohede, S., Bathgate, A.F., Llewellyn, E.J., and Degenstein, D.A. (2011): Fast NO₂ retrievals from Odin-OSIRIS limb scatter measurements, *Atmos. Meas. Tech.*, 4, 965–972, <https://doi.org/10.5194/amt-4-965-2011>
- 590
- Butler, A.H. and Domeisen, D.I.V. (2021): The wave geometry of final stratospheric warming events, *Weather Clim. Dynam.*, 2, 453–474, <https://doi.org/10.5194/wcd-2-453-2021>
- Butz, A., Bösch, H., Camy-Peyret, C., Chipperfield, M., Dorf, M., Dufour, G., Grunow, K., Jeseck, P., Kühl, S., Payan, S., Pepin, I., Pukite, J., Rozanov, A., von Savigny, C., Sioris, C., Wagner, T., Weidner, F., and Pfeilsticker, K. (2006): Inter-comparison of stratospheric O₃ and NO₂ abundances retrieved from balloon borne direct sun observations and
- 595
- Envisat/SCIAMACHY limb measurements, *Atmos. Chem. Phys.*, 6, 1293–1314, <https://doi.org/10.5194/acp-6-1293-2006>
- Callis, L.B., Russell, J.M., III, Haggard, K.V. and Natarajan, M. (1983): Examination of wintertime latitudinal gradients in stratospheric No₂ using theory and LIMS observations. *Geophys. Res. Lett.*, 10: 945-948. <https://doi.org/10.1029/GL010i010p00945>
- von Clarmann, T. (2013): Chlorine in the stratosphere. *Atmósfera*, 26 (3), 415-458, [https://doi.org/10.1016/S0187-](https://doi.org/10.1016/S0187-6236(13)71086-5)
- 600
- 6236(13)71086-5.
- Compernelle, S., Verhoelst, T., Pinardi, G., Granville, J., Hubert, D., Keppens, A., Niemeijer, S., Rino, B., Bais, A., Beirle, S., Boersma, F., Burrows, J. P., De Smedt, I., Eskes, H., Goutail, F., Hendrick, F., Lorente, A., Pazmino, A., PETERS, A., Peters, E., Pommereau, J.-P., Remmers, J., Richter, A., van Geffen, J., Van Roozendael, M., Wagner, T., and Lambert, J.-C. (2020): Validation of Aura-OMI QA4ECV NO₂ climate data records with ground-based DOAS networks: the role of
- 605
- measurement and comparison uncertainties, *Atmos. Chem. Phys.*, 20, 8017–8045, <https://doi.org/10.5194/acp-20-8017-2020>
- Cook, P.A. and Roscoe, H.K. (2009): Variability and trends in stratospheric NO₂ in Antarctic summer, and implications for stratospheric NO_y, *Atmos. Chem. Phys.*, 9, 3601–3612, <https://doi.org/10.5194/acp-9-3601-2009>

- Davies, S., Mann, G.W., Carslaw, K.S., Chipperfield, M.P., Remedios, J.J., Allen, G., Waterfall, A.M., Spang, R., and Toon, G.C. (2006): Testing our understanding of Arctic denitrification using MIPAS-E satellite measurements in winter 2002/2003, *Atmos. Chem. Phys.*, 6, 3149–3161, <https://doi.org/10.5194/acp-6-3149-2006>.
- Dessler, A. (2000), *Chemistry and Physics of Stratospheric Ozone*, Elsevier, ISBN 9780080500966.
- Dirksen, R.J., Boersma, K.F., Eskes, H.J., Ionov, D.V., Bucsela, E.J., Levelt, P.F. and Kelder, H.M. (2011): Evaluation of stratospheric NO₂ retrieved from the Ozone Monitoring Instrument: Intercomparison, diurnal cycle, and trending, *J. Geophys. Res.* 116, D08305, 22 pp., <https://doi.org/10.1029/2010JD014943>
- Dubé, K., Randel, W., Bourassa, A., Zawada, D., McLinden, C., and Degenstein, D. (2020): Trends and variability in stratospheric NO_x derived from merged SAGE II and OSIRIS satellite observations. *Journal Geophysical Research: Atmospheres*, 125, e2019JD031798. <https://doi.org/10.1029/2019JD031798>
- Dubé, K., Bourassa, A., Zawada, D., Degenstein, D., Damadeo, R., Flittner, D., and Randel, W. (2021): Accounting for the photochemical variation in stratospheric NO₂ in the SAGE III/ISS solar occultation retrieval, *Atmos. Meas. Tech.*, 14, 557–566, <https://doi.org/10.5194/amt-14-557-2021>
- Errera, Q., and D. Fonteyn (2001), Four-dimensional variational chemical assimilation of CRISTA stratospheric measurements, *J. Geophys. Res.*, 106(D11), 12253–12265, doi:10.1029/2001JD900010
- Eskes, H., van Velthoven, P., Valks, P. and Kelder, H. (2003): Assimilation of GOME total ozone satellite observations in a three-dimensional tracer transport model, *Q.J.R. Meteorol. Soc.* 129, 1663-1681, v/10.1256/qj.02.14
- Eskes, H.J. and Eichmann K.-U. (2022): S5P MPC Product Readme Nitrogen Dioxide, Report S5P-MPC-KNMI-PRF-NO₂, version 2.2, 2022-07-20, ESA, <http://www.tropomi.eu/data-products/nitrogen-dioxide/> (last access: 06 Dec. 2022)
- Eskes, H. , van Geffen, J., Sneep, M., Veeffkind, P., Niemeijer, S. and Zehner, C. (2021): S5P Nitrogen Dioxide v02.03.01 intermediate reprocessing on the S5P-PAL system: Readme file Report, version 1.0, 2021-12-15, ESA, <https://data-portal.s5p-pal.com/products/NO2.html> (last access: 06 Dec. 2022)
- Eskes, H.J., van Geffen, J.H.G.M., Boersma, K.F., Eichmann K.-U., Apituley, A., Pedernana, M., Sneep, M., Veeffkind, J.P., and Loyola, D. (2021): S5P/TROPOMI Level-2 Product User Manual Nitrogen Dioxide, Report S5P-KNMI-L2-0021-MA, version 4.0.2, ESA, <http://www.tropomi.eu/data-products/nitrogen-dioxide/>
- Fahey, D.W., Murphy, D.M., Kelly, K.K., Ko, M.K.W., Proffitt, M.H., Eubank, C.S., Ferry, G.V., Loewenstein, M., and Chan, K.R. (1989): Measurements of nitric oxide and total reactive nitrogen in the Antarctic stratosphere: Observations and chemical implications, *J. Geophys. Res.*, 94 (D14), 16665– 16681, <https://doi.org/10.1029/JD094iD14p16665>
- Fahey, D., Solomon, S., Kawa, S., Lowenstein, M., Podolske, J.J., Strahan, S.E., and Chan, K.R. (1990): A diagnostic for denitrification in the winter polar stratospheres, *Nature*, 345, 698–702, <https://doi.org/10.1038/345698a0>
- Farman, J., Gardiner, B., and Shanklin, J. (1985): Large losses of total ozone in Antarctica reveal seasonal ClO_x/NO_x interaction. *Nature* 315, 207–210, <https://doi.org/10.1038/315207a0>

- France, J.L., King, M.D., Frey, M.M., Erbland, J., Picard, G., Preunkert, S., MacArthur, A., and Savarino, J. (2011): Snow optical properties at Dome C (Concordia), Antarctica; implications for snow emissions and snow chemistry of reactive nitrogen, *Atmos. Chem. Phys.*, 11, 9787–9801, <https://doi.org/10.5194/acp-11-9787-2011>.
- 645 Frey, M.M., Brough, N., France, J.L., Anderson, P.S., Traulle, O., King, M.D., Jones, A.E., Wolff, E. W., and Savarino, J. (2013): The diurnal variability of atmospheric nitrogen oxides (NO and NO₂) above the Antarctic Plateau driven by atmospheric stability and snow emissions, *Atmos. Chem. Phys.*, 13, 3045–3062, <https://doi.org/10.5194/acp-13-3045-2013>
- Frey, M.M., Roscoe, H.K., Kukui, A., Savarino, J., France, J.L., King, M.D., Legrand, M., and Preunkert, S. (2015): Atmospheric nitrogen oxides (NO and NO₂) at Dome C, East Antarctica, during the OPALE campaign, *Atmos. Chem. Phys.*, 15, 7859–7875, <https://doi.org/10.5194/acp-15-7859-2015>
- 650 Funke, B., López-Puertas, M., Gil-López, S., von Clarmann, T., Stiller, G.P., Fischer, H., and Kellmann, S. (2005): Downward transport of upper atmospheric NO_x into the polar stratosphere and lower mesosphere during the Antarctic 2003 and Arctic 2002/2003 winters, *J. Geophys. Res.*, 110, D24308, <https://doi.org/10.1029/2005JD006463>
- Garcia, R.R., and Solomon, S. (1994): A new numerical model of the middle atmosphere: 2. Ozone and related species, *J. Geophys. Res.*, 99(D6), 12937– 12951, <https://doi.org/10.1029/94JD00725>
- 655 van Geffen, J.H.G.M., Eskes, H.J., Compennolle, S., Pinardi, G., Verhoelst, T., Lambert, J.-C., Sneep, M., ter Linden, M., Ludewig, A., Boersma, K.F. and Veefkind, J.P.: Sentinel-5P TROPOMI NO₂ retrieval (2022a): impact of version v2.2 improvements and comparisons with OMI and ground-based data, *Atmos. Meas. Tech.*, 15, 2037-2060, <https://doi.org/10.5194/amt15-2037-2022>, 2022a.
- van Geffen, J.H.G.M., Eskes, H.J., Boersma, K.F., and Veefkind, J.P. (2022b): TROPOMI ATBD of the total and tropospheric NO₂ data products, Report S5P-KNMI-L2-0005-RP, version 2.4.0, 202207-11, KNMI, De Bilt, The Netherlands, <http://www.tropomi.eu/data-products/nitrogen-dioxide/> (last access: 06 Dec. 2022)
- 660 Gil, M., and Cacho, J. (1992): NO₂ total column evolution during the 1989 spring at Antarctica Peninsula. *J Atmos Chem* 15, 187–200, <https://doi.org/10.1007/BF00053759>
- Goldman, A., Fernald, F.A., Williams, W.J., and Murcray, D.G. (1978), Vertical distribution of NO₂ in the stratosphere as determined from balloon measurements of solar spectra in the 4500Å region, *Geophys. Res. Lett.*, 5, 257, <https://doi.org/10.1029/GL005i004p00257>
- 665 Gordon, E.M., Seppälä, A., and Tamminen, J. (2020): Evidence for energetic particle precipitation and quasi-biennial oscillation modulations of the Antarctic NO₂ springtime stratospheric column from OMI observations, *Atmos. Chem. Phys.*, 20, 6259–6271, <https://doi.org/10.5194/acp-20-6259-2020>
- 670 Haley, C., Brohede, S., Sioris, C., Griffioen, E., Murtagh, D., Mcdade, I., Eriksson, P., Llewellyn, E., Bazureau, A., and Goutail, F. (2004): Retrieval of stratospheric O₃ and NO₂ profiles from Odin Optical Spectrograph and Infrared Imager System (OSIRIS) limb-scattered sunlight measurements. *Journal of Geophysical Research*, 109, D16303, <https://doi.org/10.1029/2004JD004588>

- 675 Hendrick, F., Barret, B., Van Roozendael, M., Boesch, H., Butz, A., De Mazière, M., Goutail, F., Hermans, C., Lambert, J.-
C., Pfeilsticker, K., and Pommereau, J.-P. (2004): Retrieval of nitrogen dioxide stratospheric profiles from ground-based
zenith-sky UV-visible observations: validation of the technique through correlative comparisons, *Atmos. Chem. Phys.*, 4,
2091–2106, <https://doi.org/10.5194/acp-4-2091-2004>
- 680 Hendrick, F., Pommereau, J.-P., Goutail, F., Evans, R.D., Ionov, D., Pazmino, A., Kyrö, E., Held, G., Eriksen, P., Dorokhov,
V., Gil, M., and Van Roozendael, M. (2011): NDACC/SAOZ UV-visible total ozone measurements: improved retrieval
and comparison with correlative ground-based and satellite observations, *Atmos. Chem. Phys.*, 11, 5975–5995,
<https://doi.org/10.5194/acp-11-5975-2011>
- 685 Hilboll, A., Richter, A., Rozanov, A., Hodnebrog, Ø., Heckel, A., Solberg, S., Stordal, F., and Burrows, J.P. (2013):
Improvements to the retrieval of tropospheric NO₂ from satellite – stratospheric correction using SCIAMACHY limb/nadir
matching and comparison to Oslo CTM2 simulations, *Atmos. Meas. Tech.*, 6, 565–584, <https://doi.org/10.5194/amt-6-565-2013>
- Hoffmann, L., Rößler, T., Stein, O., Wu, X., and Hertzog, A. (2017): Intercomparison of meteorological analyses and
trajectories in the Antarctic lower stratosphere with Concordiasi superpressure balloon observations. *Atmospheric
Chemistry & Physics*, 17(13), 8045–8061, <https://doi.org/10.5194/acp-17-8045-2017>
- 690 Hoor, P., Fischer, H., Lange, L., Lelieveld, J., and Brunner, D. (2002): Seasonal variations of a mixing layer in the
lowermost stratosphere as identified by the CO-O₃ correlation from in situ measurements, *J. Geophys. Res.*, 107(D5),
<https://doi.org/10.1029/2000JD000289>
- Hurwitz, M.M., Fleming, E.L., Newman, P.A., Li, F., Mlawer, E., Cady-Pereira, K., and Bailey, R. (2015): Ozone depletion
by hydrofluorocarbons, *Geophys. Res. Lett.*, 42, 8686–8692, <https://doi.org/10.1002/2015GL065856>
- 695 Joseph, B., and B. Legras (2002), Relation between Kinematic Boundaries, Stirring, and Barriers for the Antarctic Polar
Vortex. *J. Atmos. Sci.*, 59, 1198–1212, doi:10.1175/1520-0469(2002)059<1198:RBKBSA>2.0.CO;2.
- 700 Kerzenmacher, T., Wolff, M.A., Strong, K., Dupuy, E., Walker, K.A., Amekudzi, L.K., Batchelor, R. L., Bernath, P.F.,
Berthet, G., Blumenstock, T., Boone, C.D., Bramstedt, K., Brogniez, C., Brohede, S., Burrows, J.P., Catoire, V., Dodion,
J., Drummond, J.R., Dufour, D.G., Funke, B., Fussen, D., Goutail, F., Griffith, D.W.T., Haley, C.S., Hendrick, F.,
Höpfner, M., Huret, N., Jones, N., Kar, J., Kramer, I., Llewellyn, E.J., López-Puertas, M., Manney, G., McElroy, C.T.,
McLinden, C.A., Melo, S., Mikuteit, S., Murtagh, D., Nichitiu, F., Notholt, J., Nowlan, C., Piccolo, C., Pommereau, J.-P.,
Randall, C., Raspollini, P., Ridolfi, M., Richter, A., Schneider, M., Schrems, O., Silicani, M., Stiller, G.P., Taylor, J.,
Tétard, C., Toohey, M., Vanhellefont, F., Warneke, T., Zawodny, J.M., and Zou, J. (2008): Validation of NO₂ and NO
from the Atmospheric Chemistry Experiment (ACE), *Atmos. Chem. Phys.*, 8, 5801–5841, <https://doi.org/10.5194/acp-8-5801-2008>.
- 705 Khaykin, S., Legras, B., Bucci, S., Sellitto, P., Isaksen, L., Tencé, F., Bekki, S., Bourassa, A., Rieger, L., Zawada, D.,
Jumelet, J., and Godin-Beekmann, S. (2020): The 2019/20 Australian wildfires generated a persistent smoke-charged

- vortex rising up to 35 km altitude. *Communications Earth & Environment*, 1(1), 1– 12, <https://doi.org/10.1038/s43247-020-00022-5>
- 710 Khaykin, S.M., de Laat, A.T.J., Godin-Beekmann, S., Hauchecorne, A., and M. Ratynski (2022): Unexpected self-lofting and dynamical confinement of volcanic plumes: the Raikoke 2019 case. *Sci Rep* 12, 22409 <https://doi.org/10.1038/s41598-022-27021-0>
- Khosrawi, F., Urban, J., Pitts, M.C., Voelger, P., Achtert, P., Kaphlanov, M., Santee, M.L., Manney, G. L., Murtagh, D., and Fricke, K.-H. (2011): Denitrification and polar stratospheric cloud formation during the Arctic winter 2009/2010, *Atmos. Chem. Phys.*, 11, 8471–8487, <https://doi.org/10.5194/acp-11-8471-2011>
- 715 Khosrawi, F., Kirner, O., Sinnhuber, B.-M., Johansson, S., Höpfner, M., Santee, M.L., Froidevaux, L., Ungermann, J., Ruhnke, R., Woiwode, W., Oelhaf, H., and Braesicke, P. (2017): Denitrification, dehydration and ozone loss during the 2015/2016 Arctic winter, *Atmos. Chem. Phys.*, 17, 12893–12910, <https://doi.org/10.5194/acp-17-12893-2017>
- Koh, T.Y., and Legras, B. (2002); Hyperbolic lines and the stratospheric polar vortex, *Chaos*, 1 June 2002, 12 (2), 382–394, <https://doi.org/10.1063/1.1480442>
- 720 Kondo, Y., Matthews, W.A., Solomon, S., Koike, M., Hayashi, M., Yamazaki, K., Nakajima, H., and Tsukui, K. (1994): Ground-based measurements of column amounts of NO₂ over Syowa Station, Antarctica, *J. Geophys. Res.*, 99(D7), 14535– 14548, <https://doi.org/10.1029/94JD00403>
- Krasauskas, L., Ungermann, J., Preusse, P., Friedl-Vallon, F., Zahn, A., Ziereis, H., Rolf, C., Plöger, F., Konopka, P., Vogel, B., and Riese, M. (2021): 3-D tomographic observations of Rossby wave breaking over the North Atlantic during the WISE aircraft campaign in 2017, *Atmos. Chem. Phys.*, 21, 10249–10272, <https://doi.org/10.5194/acp-21-10249-2021>.
- 725 Kritten, L., Butz, A., Dorf, M., Deutschmann, T., Kühl, S., Prados-Roman, C., Puķīte, J., Rozanov, A., Schofield, R., and Pfeilsticker, K. (2010): Time dependent profile retrieval of UV/vis absorbing radicals from balloon-borne limb measurements – a case study on NO₂ and O₃, *Atmos. Meas. Tech.*, 3, 933–946, <https://doi.org/10.5194/amt-3-933-2010>
- Krotkov N, Realmuto, V., Li, C., Seftor, C., Li, J., Brentzel, K., Stuefer, M., Cable, J., Dierking, C., Delamere, J., Schneider, D., Tamminen, J., Hassinen, S., Ryppö, T., Murray, J., Carn, S., Osiensky, J., Eckstein, N., Layne, G., and Kirkendall, J. (2021): Day–Night Monitoring of Volcanic SO₂ and Ash Clouds for Aviation Avoidance at Northern Polar Latitudes. *Remote Sensing*. 13(19):4003, <https://doi.org/10.3390/rs13194003>
- 730 Kühl, S., Wilms-Grabe, W., Frankenberg, C., Grzegorski, M., Platt, U., and Wagner, T. (2006): Comparison of OClO nadir measurements from SCIAMACHY and GOME, *Adv. Space Res.*, 37, 2247–2253, <https://doi.org/10.1016/j.asr.2005.06.061>
- 735 Kühl, S., Pukite, J., Deutschmann, T., Platt, U., and Wagner, T. (2008): SCIAMACHY limb measurements of NO₂, BrO and OClO. Retrieval of vertical profiles: Algorithm, first results, sensitivity and comparison studies, *Advances in Space Research*, 42(10), 1747-1764
- 740 de Laat, A., van Weele, M. (2011): The 2010 Antarctic ozone hole: Observed reduction in ozone destruction by minor sudden stratospheric warmings. *Sci Rep* 1, 38), <https://doi.org/10.1038/srep00038>

- Lambert, J.-C., Compernelle, S., Eichmann, K.-U., de Graaf, M., Hubert, D., Keppens, A., Kleipool, Q., Langerock, B., Sha, M.K., Verhoelst, T., Wagner, T., Ahn, C., Argyrouli, A., Balis, D., Chan, K.L., De Smedt, I., Eskes, H., Fjæraa, A. M., Garane, K., Gleason, J.F., Goutail, F., Granville, J., Hedelt, P., Heue, K.-P., Jaross, G., Koukouli, M.-L., Landgraf, J., Lutz, R., Nanda, S., Niemeijer, S., Pazmiño, A., Pinardi, G., Pommereau, J.-P., Richter, A., Rozemeijer, N., Sneep, M., Stein Zweers, D., Theys, N., Tilstra, G., Torres, O., Valks, P., van Geffen, J., Vigouroux, C., Wang, P. and Weber, M. (2023): Quarterly Validation Report of the Copernicus Sentinel-5 Precursor Operational Data Products, #16: April 2018 – August 2022, S5P MPC Routine Operations Consolidated Validation Report series, Issue 16.01.00, 189 pp., 2022-09-23, <http://mpc-vdaf.tropomi.eu/index.php/nitrogen-dioxide/> (last access: June 2023)
- 745 Lecouffe, A., Godin-Beekmann, S., Pazmiño, A., and Hauchecorne, A. (2022): Evolution of the intensity and duration of the Southern Hemisphere stratospheric polar vortex edge for the period 1979–2020, *Atmos. Chem. Phys.*, 22, 4187–4200, <https://doi.org/10.5194/acp-22-4187-2022>
- 750 de Leeuw, J., Schmidt, A., Witham, C.S., Theys, N., Taylor, I.A., Grainger, R.G., Pope, R.J., Haywood, J., Osborne, M., and Kristiansen, N.I. (2021): The 2019 Raikoke volcanic eruption – Part 1: Dispersion model simulations and satellite retrievals of volcanic sulfur dioxide, *Atmos. Chem. Phys.*, 21, 10851–10879, <https://doi.org/10.5194/acp-21-10851-2021>
- 755 Lindenmaier, R., Strong, K., Batchelor, R.L., Bernath, P.F., Chabrillat, S., Chipperfield, M.P., Daffer, W. H., Drummond, J.R., Feng, W., Jonsson, A.I., Kolonjari, F., Manney, G.L., McLinden, C., Ménard, R., and Walker, K.A. (2011): A study of the Arctic NO_y budget above Eureka, Canada, *J. Geophys. Res.*, 116, D23302, <https://doi.org/10.1029/2011JD016207>
- Magaritz-Ronen, L., and Raveh-Rubin, S. (2021): Wildfire smoke highlights troposphere-to-stratosphere pathway. *Geophysical Research Letters*, 48, e2021GL095848. <https://doi.org/10.1029/2021GL095848>
- 760 Maliniemi, V., Nesse Tysøy, H., Smith-Johnsen, C., Arsenovic, P., and Marsh, D.R. (2021): Effects of enhanced downwelling of NO_x on Antarctic upper-stratospheric ozone in the 21st century, *Atmos. Chem. Phys.*, 21, 11041–11052, <https://doi.org/10.5194/acp-21-11041-2021>
- Manney, G.L., Santee, M.L., Livesey, N.J., Froidevaux, L., Read, W.G., Pumphrey, H.C., Waters, J.W., and Pawson, S. (2005): EOS Microwave Limb Sounder observations of the Antarctic polar vortex breakup in 2004, *Geophys. Res. Lett.*, 32, L12811, doi:10.1029/2005GL022823
- 765 Mount, G.H., Rusch, D.W., Noxon, J.F., Zawodny, J.M., and Barth, C.A. (1984): Measurements of stratospheric NO₂ from the Solar Mesosphere Explorer satellite: 1. An overview of the results, *J. Geophys. Res.*, 89 (D1), 1327– 1340, doi:10.1029/JD089iD01p01327
- Müller, R. (2021): The impact of the rise in atmospheric nitrous oxide on stratospheric ozone. *Ambio* 50, 35–39, <https://doi.org/10.1007/s13280-020-01428-3>
- 770 Müller, R., Grooß, J.-U., Lemmen, C., Heinze, D., Dameris, M., and Bodeker, G. (2008): Simple measures of ozone depletion in the polar stratosphere, *Atmos. Chem. Phys.*, 8, 251–264, <https://doi.org/10.5194/acp-8-251-2008>

- Munro, R., Eisinger, M., Anderson, C., Callies, J., Corpaccioli, E. Lang, R., Lefebvre, A., Livschitz, Y. and Albinana (2006), GOME-2 on MetOp, Proceedings of the 2006 EUMETSAT Meteorological Satellite Conference, Helsinki, Finland. Vol. 775 1216, ESA publication SP 628, Paris, 2006
- Munro, R., Lang, R., Klaes, D., Poli, G., Retscher, C., Lind-strot, R., Huckle, R., Lacan, A., Grzegorski, M., Holdak, A.,Kokhanovsky, A., Livschitz, J. and Eisinger, M. (2016): The GOME-2 instrument on the Metop series of satellites: instrument design, calibration, and level 1 data processing – an overview, *Atmos. Meas. Tech.*, 9, 1279-1301, <https://doi.org/10.5194/amt-9-1279-2016>,
- 780 Newman, P.A., Lait , L.R., Schoeberl, M.R., Seablom, M., Coy, L., Rood, R., Swinbank, R., Proffitt, M., Loewenstein, M., Podolske, J.R., Elkins, J.W., Webster, C.R., May, R.D., Fahey, D.W., Dutton, G.S., and Chan, K.R. (1996), Measurements of polar vortex air in the midlatitudes, *J. Geophys. Res.*, 101 (D8), 12879 <https://doi.org/10.1029/95JD03387>.
- Noxon, J.F. (1978): Stratospheric NO₂ in the Antarctic winter. *Geophys. Res. Lett.*, 5, 1021-1022, <https://doi.org/10.1029/GL005i012p01021>
- 785 Noxon, J.F. (1979): Stratospheric NO₂: 2. Global behavior, *J. Geophys. Res.* 84 (C8), 5067-5076, <https://doi.org/10.1029/JC084iC08p05067>
- Oetjen, H., Wittrock, F., Richter, A., Chipperfield, M.P., Medeke, T., Sheode, N., Sinnhuber, B.-M., Sinnhuber, M., and Burrows, J.P. (2011): Evaluation of stratospheric chlorine chemistry for the Arctic spring 2005 using modelled and measured OClO column densities, *Atmos. Chem. Phys.*, 11, 689–703, <https://doi.org/10.5194/acp-11-689-2011>
- 790 Oppenheimer, C., Kyle, P.R., Tsanev, V.I., McGonigle, A.J.S., Mather, T.A. and Sweeney, D., (2005): Mt. Erebus, the largest point source of NO₂ in Antarctica. *Atmospheric Environment*, 39 (32), pp.6000-6006, <https://doi.org/10.1016/j.atmosenv.2005.06.036>
- Orsolini, Y.J., and Grant, W.B. (2000): Seasonal formation of nitrous oxide laminae in the mid and low latitude stratosphere. *Geophysical research letters*, 27(8), 1119-1122. <https://doi.org/10.1029/95JD03387>.
- 795 Pinardi, G., Van Roozendaal, M., Hendrick, F., Richter, A., Valks, P., Alwarda, R., Bogner, K., Frieß, U., Granville, J., Gu, M., Johnston, P., Prados-Roman, C., Querel, R., Strong, K., Wagner, T., Wittrock, F., and Yela Gonzalez, M. (2022): Ground-based validation of the MetOp-A and MetOp-B GOME-2 OClO measurements, *Atmos. Meas. Tech.*, 15, 3439–3463, <https://doi.org/10.5194/amt-15-3439-2022>
- Plumb, R.A. (2007): Tracer interrelationships in the stratosphere, *Rev. Geophys.*, 45, RG4005, 800 <https://doi.org/10.1029/2005RG000179>.
- Pommereau, J. P., and Goutail, F. (1988): O₃ and NO₂ ground-based measurements by visible spectrometry during Arctic winter and spring 1988. *Geophysical Research Letters*, 15(8), 891-894, <https://doi.org/10.1029/GL015i008p00891>
- Puķīte, J., Borger, C., Dörner, S., Gu, M., Frieß, U., Meier, A.C., Enell, C.-F., Raffalski, U., Richter, A., and Wagner, T. (2021): Retrieval algorithm for OClO from TROPOMI (TROPOspheric Monitoring Instrument) by differential optical 805 absorption spectroscopy, *Atmos. Meas. Tech.*, 14, 7595–7625, <https://doi.org/10.5194/amt-14-7595-2021>

- Randall, C.E., Rusch, D.W., Bevilacqua, R.M., Hoppel, K.W., and Lumpe, J.D. (1998): Polar Ozone and Aerosol Measurement (POAM) II stratospheric NO₂, 1993–1996, *J. Geophys. Res.*, 103(D21), 28361– 28371, <https://doi.org/10.1029/98JD02092>
- 810 P. Ricaud, Lefèvre, F., Berthet, G., Murtagh, D., Llewellyn, E.J., Mégie, G., Kyrölä, E., Leppelmeier, G.W., Auvinen, H., Boone, C., Brohede, S., Degenstein, D.A., de La Noë, J., Dupuy, E., El Amraoui, L., Eriksson, P., Evans, W.F.J., Frisk, U., Gattinger, R.L., Girod, F., Haley, C.S., Hassinen, S., Hauchecorne, A., Jimenez, C., Kyrö, E., Lantié, N., Le Flochmoën, E., Lloyd, N.D., McConnell, J.C., McDade, I.C., Nordh, L., Olberg, M., Pazmino, A., Petelina, S.V., Sandqvist, A., Seppälä, A., Sioris, C.E., Solheim, B.H., Stegman, J., Strong, K., Taalas, P., Urban, J., von Savigny, C., von Scheele, F., and Witt, G. (2005): Polar vortex evolution during the 2002 Antarctic major warming as observed by the Odin
815 satellite, *J. Geophys. Res.*, 110, D05302, <https://doi.org/10.1029/2004JD005018>
- Richter, A., Wittrock, F., Weber, M., Beirle, S., Kühl, S., Platt, U., Wagner, T., Wilms-Grabe, W. and Burrows, J.P. (2005). GOME observations of stratospheric trace gas distributions during the splitting vortex event in the Antarctic winter of 2002. Part I: Measurements. *Journal of the atmospheric sciences*, 62(3), 778-785, <https://doi.org/10.1175/JAS-3325.1>
- 820 Ridley, B.A., Luu, S.H., Hastie, D.R., Schiff, H.I., McConnell, J.C., Evans, W.F. J., McElroy, C.T., Kerr, J.B., Fast, H., and O'Brien, R.S. (1984): Stratospheric odd nitrogen: Measurements of HNO₃, NO, NO₂, and O₃ near 54°N in winter, *J. Geophys. Res.*, 89(D3), 4797–4820, doi:10.1029/JD089iD03p04797
- Rinsland, C.P., Gunson, M.R., Salawitch, R.J., Michelsen, H.A., Zander, R., Newchurch, M.J., Abbas, M.M., Abrams, M.C., Manney, G.L., Chang, A.Y., Irion, F.W., Goldman, A., and Mahieu, E. (1996): ATMOS/ATLAS-3 measurements of stratospheric chlorine and reactive nitrogen partitioning inside and outside the November 1994 Antarctic vortex.
825 *Geophysical research letters*, 23(17), 2365-2368, <https://doi.org/10.1029/96GL01474>
- Ronsmans, G., Langerock, B., Wespes, C., Hannigan, J.W., Hase, F., Kerzenmacher, T., Mahieu, E., Schneider, M., Smale, D., Hurtmans, D., De Mazière, M., Clerbaux, C., and Coheur, P.-F. (2016): First characterization and validation of FORLI-HNO₃ vertical profiles retrieved from IASI/Metop, *Atmos. Meas. Tech.*, 9, 4783–4801, <https://doi.org/10.5194/amt-9-4783-2016>
- 830 Russell, J.M., Solomon, S., Gordley, L.L., Remsberg, E.E., and Callis, L.B. (1984): The variability of stratospheric and mesospheric NO₂ in the polar winter night observed by LIMS, *J. Geophys. Res.*, 89(D5), 7267– 7275, doi:10.1029/JD089iD05p07267
- Stone, K.A., Solomon, S., Kinnison, D.E., and Mills, M.J. (2021): On recent large Antarctic ozone holes and ozone recovery metrics. *Geophysical Research Letters*, 48, e2021GL095232. <https://doi.org/10.1029/2021GL095232>
- 835 Salawitch, R., Gobbi, G., Wofsy, S., and McElroy, M.B. (1989): Denitrification in the Antarctic stratosphere, *Nature*, 339, 525–527, <https://doi.org/10.1038/339525a0>
- Santee, M.L., MacKenzie, I.A., Manney, G.L., Chipperfield, M.P., Bernath, P.F., Walker, K.A., Boone, C.D., Froidevaux, L., Livesey, N.J., and Waters, J.W. (2008): A study of stratospheric chlorine partitioning based on new satellite measurements and modeling, *J. Geophys. Res.*, 113, D12307, <https://doi.org/10.1029/2007JD009057>

- 840 Sato, K., Tomikawa, Y., Hashida, G., Yamanouchi, T., Nakajima, H., and Sugita, T. (2009): Longitudinally Dependent Ozone Increase in the Antarctic Polar Vortex Revealed by Balloon and Satellite Observations, *J. Atmos. Sci.*, 66, 1807–1820, <https://doi.org/10.1175/2008JAS2904.1>.
- Schoeberl, M.R., Lait, L.R., Newman, P.A., and Rosenfield, J.E. (1992): The structure of the polar vortex, *J. Geophys. Res.*, 97 (D8), 7859– 7882, <https://doi.org/10.1029/91JD02168>
- 845 Sanders, R.W., Solomon, S., Kreher, K., and Johnston, P.V. (1999): An Intercomparison of NO₂ and OClO Measurements at Arrival Heights, Antarctica during Austral Spring 1996. *Journal of Atmospheric Chemistry* 33, 283–298, <https://doi.org/10.1023/A:1006185027584>
- von Savigny, C., Rozanov, A., Bovensmann, H., Eichmann, K.-U., Noel, S., Rozanov, V. V., Sinnhuber, B.-M., Weber, M., Burrows, J. P., and Kaiser, J. (2005): The ozone hole break-up in September 2002 as seen by SCIAMACHY on
- 850 ENVISAT, *J. Atmos. Sci.*, 62, 721–734, <https://doi.org/10.1175/JAS-3328.1>
- Smale, D., Strahan, S.E., Querel, R., Frieß, U., Nedoluha, G.E., Nichol, S.E., Robinson, J., Boyd, I., Kotkamp, M., Gomez, R.M., Murphy, M., Tran, H., and McGaw, J. (2021): Evolution of observed ozone, trace gases, and meteorological variables over Arrival Heights, Antarctica (77.8°S, 166.7°E) during the 2019 Antarctic stratospheric sudden warming, *Tellus B: Chemical and Physical Meteorology*, 73:1, 1-18, <https://doi.org/10.1080/16000889.2021.1933783>
- 855 Sofieva, V.F., Kalakoski, N., Verronen, P.T., Päivärinta, S.-M., Kyrölä, E., Backman, L., and Tamminen, J. (2012): Polar-night O₃, NO₂ and NO₃ distributions during sudden stratospheric warmings in 2003–2008 as seen by GOMOS/Envisat, *Atmos. Chem. Phys.*, 12, 1051–1066, <https://doi.org/10.5194/acp-12-1051-2012>
- Solomon, S., and Garcia, R.R. (1983): On the distribution of nitrogen dioxide in the high-latitude stratosphere, *J. Geophys. Res.*, 88(C9), 5229– 5239, <https://doi.org/10.1029/JC088iC09p05229>
- 860 Solomon, S. (1990): Nitrogen chemistry in Antarctica: A brief review. *Dynamics, Transport and Photochemistry in the Middle Atmosphere of the Southern Hemisphere*, NATO ASI Series book series (ASIC) volume 321, 191-201
- Solomon, S., and Keys, J.G. (1992): Seasonal variations in Antarctic NO_x chemistry, *J. Geophys. Res.*, 97(D8), 7971–7978, <https://doi.org/10.1029/91JD01707>
- Solomon, S., Ivy, D.J., Kinnison, D., Mills, M.J., Neely III, R.R., and Schmidt, A. (2016): Emergence of healing in the
- 865 Antarctic ozone layer, *Science*, 353, 269-274, <https://doi.org/10.1126/science.aae0061>
- Solomon, S., Smith, J.P., Sanders, R.W., Perliski, L., Miller, H.L., Mount, G.H., Keys, J.G., and Schmeltekopf, A.L. (1993): Visible and near-ultraviolet spectroscopy at McMurdo Station, Antarctica: 8. Observations of nighttime NO₂ and NO₃ from April to October 1991, *J. Geophys. Res.*, 98(D1), 993– 1000, <https://doi.org/10.1029/92JD02390>
- Stone, K.A., Solomon, S., Kinnison, D.E., and Mills, M.J. (2021): On recent large Antarctic ozone holes and ozone recovery
- 870 metrics. *Geophysical Research Letters*, 48, e2021GL095232. <https://doi.org/10.1029/2021GL095232>
- Strahan, S.E., Douglass, A.R., Newman, P.A., and Steenrod, S.D. (2014): Inorganic chlorine variability in the Antarctic vortex and implications for ozone recovery, *J. Geophys. Res. Atmos.*, 119, 14,098– 14,109, <https://doi.org/10.1002/2014JD022295>

- 875 Strahan, S.E., Douglass, A.R., and Damon, M.R. (2019): Why do Antarctic ozone recovery trends vary?. *Journal of Geophysical Research: Atmospheres*, 124, 8837 – 8850. <https://doi.org/10.1029/2019JD030996>
- Strode, S.A., Taha, G., Oman, L.D., Damadeo, R., Flittner, D., Schoeberl, M., Sioris, C.E., and Stauffer, R. (2022): SAGE III/ISS ozone and NO₂ validation using diurnal scaling factors, *Atmos. Meas. Tech.*, 15, 6145–6161, <https://doi.org/10.5194/amt-15-6145-2022>
- 880 Struthers, H., Kreher, K., Austin, J., Schofield, R., Bodeker, G., Johnston, P., Shiona, H., and Thomas, A. (2004): Past and future simulations of NO₂ from a coupled chemistry-climate model in comparison with observations, *Atmos. Chem. Phys.*, 4, 2227–2239, <https://doi.org/10.5194/acp-4-2227-2004>
- Tabazadeh, A., Santee, M.L., Danilin, M.Y., Pumphrey, H.C., Newman, P.A., Hamill, P.J., and Mergenthaler, J.L. (2000): Quantifying Denitrification and Its Effect on Ozone Recovery, *Science* 288, 1407-1411, <https://doi.org/10.1126/science.288.5470.1407>
- 885 Toon, G.C., Farmer, C.B., Lowes, L.L., Schaper, P.W., Blavier, J.-F., and Norton, R.H. (1989): Infrared aircraft measurements of stratospheric composition over Antarctica during September 1987, *J. Geophys. Res.*, 94(D14), 16571–16596, doi:10.1029/JD094iD14p16571
- Valks, P., Pinardi, G., Richter, A., Lambert, J.-C., Hao, N., Loyola, D., Van Roozendael, M., and Emmadi, S. (2011): Operational total and tropospheric NO₂ column retrieval for GOME-2, *Atmos. Meas. Tech.*, 4, 1491–1514, <https://doi.org/10.5194/amt-4-1491-2011>
- 890 van Geffen, J., Van Weele, M., Allaart, M. and Van der A, R. (2017): TEMIS UV index and UV dose operational data products, version 2, Royal Netherlands Meteorological Institute (KNMI), Dataset, <https://doi.org/10.21944/temis-uv-oper-v2>
- van Geffen, J.H.G.M., Boersma, K.F., Eskes, H.J., Sneep, M., ter Linden, M., Zara, M. and Veefkind, J.P. (2020): S5P/TROPOMI NO₂ slant column retrieval: method, stability, uncertainties and comparisons with OMI, *Atmos. Meas. Tech.*, 13, 1315-1335, <https://doi.org/10.5194/amt-13-1315-2020>,
- 895 Veefkind, J.P., Aben, I., McMullan, K., Förster, H., de Vries, J., Otter, G., Claas, J., Eskes, H.J., de Haan, J.F., Kleipool, Q., van Weele, M., Hasekamp, O., Hoogeveen, R., Landgraf, J., Snel, R., Tol, P., Ingmann, P., Voors, R., Kruizinga, B., Vink, R., Visser, H. and Levelt, P.F. (2012): TROPOMI on the ESA Sentinel-5 Precursor: A GMES mission for global observations of the atmospheric composition for climate, air quality and ozone layer applications, *Rem. Sens. Environment*, 120, 70-83, <https://doi.org/10.1016/j.rse.2011.09.027>
- 900 Veefkind, P. and Loyola, D. (2022): S5P/TROPOMI Level-2 Product User Manual Nitrogen Dioxide, Report S5P-KNMI-L2-0021-MA, version 4.1.0, 2022-07-11, ESA, <http://www.tropomi.eu/data-products/nitrogen-dioxide/> (last access: 06 Dec. 2022)
- 905 Verhoelst, T., Compernelle, S., Pinardi, G., Lambert, J.-C., Eskes, H. J., Eichmann, K.-U., Fjæraa, A.M., Granville, J., Niemeijer, S., Cede, A., Tiefengraber, M., Hendrick, F., Pazmiño, A., Bais, A., Bazureau, A., Boersma, K.F., Bognar, K., Dehn, A., Donner, S., Elokhov, A., Gebetsberger, M., Goutail, F., Grutter de la Mora, M., Gruzdev, A., Gratsea, M.,

- Hansen, G.H., Irie, H., Jepsen, N., Kanaya, Y., Karagkiozidis, D., Kivi, R., Kreher, K., Levelt, P.F., Liu, C., Müller, M., Navarro Comas, M., Piters, A.J.M., Pommereau, J.-P., Portafaix, T., Prados-Roman, C., Puentedura, O., Querel, R., Remmers, J., Richter, A., Rimmer, J., Rivera Cárdenas, C., Saavedra de Miguel, L., Sinyakov, V.P., Stremme, W., Strong, K., Van Roozendaal, M., Veefkind, J.P., Wagner, T., Wittrock, F., Yela González, M., and Zehner, C. (2021): Ground-based validation of the Copernicus Sentinel-5P TROPOMI NO₂ measurements with the NDACC ZSL-DOAS, MAX-DOAS and Pandonia global networks, *Atmos. Meas. Tech.*, 14, 481–510, <https://doi.org/10.5194/amt-14-481-2021>
- Wargan, K., Weir, B., Manney, G.L., Cohn, S.E., and Livesey, N.J. (2020): The anomalous 2019 Antarctic ozone hole in the GEOS Constituent Data Assimilation System with MLS observations, *J. of Geoph. Res. Atm.*, 125, e2020JD033335. <https://doi.org/10.1029/2020JD033335>
- Waugh, D.W., and Plumb, R.A. (1994): Contour advection with surgery: A technique for investigating finescale structure in tracer transport, *Journal of atmospheric sciences*, 51 (4), 530-540, [https://doi.org/10.1175/1520-0469\(1994\)051<0530:CAWSAT>2.0.CO;2](https://doi.org/10.1175/1520-0469(1994)051<0530:CAWSAT>2.0.CO;2)
- Waugh, D.W., and Polvani, L.M. (2010), Stratospheric polar vortices. in: *The Stratosphere: Dynamics, Transport, and Chemistry*, L M. Polvani (Editor), A.H. Sobel (Editor), D.W. Waugh (Editor), ISBN: 978-0-875-90479-5
- Weimer, M., Kinnison, D.E., Wilka, C., and Solomon, S. (2022): Effects of denitrification on the distributions of trace gas abundances in the polar regions: a model-data comparison, *EGUsphere* (preprint), doi: 10.5194/egusphere-2022-1422
- Wenig, M., Kuhl, S., Beirle, S., Bucsela, E., Jähne, B., Platt, U., Gleason, J., and Wagner, T. (2004): Retrieval and analysis of stratospheric NO₂ from the Global Ozone Monitoring Experiment, *J. Geophys. Res.*, 109, D04315, <https://doi.org/10.1029/2003JD003652>.
- Wespes, C., Hurtmans, D., Clerbaux, C., Santee, M.L., Martin, R.V., and Coheur, P.F. (2009), Global distributions of nitric acid from IASI/MetOP measurements, *Atmos. Chem. Phys.*, 9, 7949–7962, <https://doi.org/10.5194/acp-9-7949-2009>
- Wespes, C., Ronsmans, G., Clarisse, L., Solomon, S., Hurtmans, D., Clerbaux, C., and Coheur, P.-F. (2022): Polar stratospheric nitric acid depletion surveyed from a decadal dataset of IASI total columns, *Atmos. Chem. Phys.*, 22, 10993–11007, <https://doi.org/10.5194/acp-22-10993-2022>
- Yela, M., Parrondo, C., Gil, M., Rodríguez, S., Araujo, J., Ochoa, H., Deferrari, G., and Díaz, S. (2005): The September 2002 Antarctic vortex major warming as observed by visible spectroscopy and ozone soundings, *International Journal of Remote Sensing*, 26:16, 3361-3376, <https://doi.org/10.1080/01431160500076285>
- Yela, M., Gil-Ojeda, M., Navarro-Comas, M., Gonzalez-Bartolomé, D., Puentedura, O., Funke, B., Iglesias, J., Rodríguez, S., García, O., Ochoa, H., and Deferrari, G. (2017): Hemispheric asymmetry in stratospheric NO₂ trends, *Atmos. Chem. Phys.*, 17, 13373–13389, <https://doi.org/10.5194/acp-17-13373-2017>
- Zempila, M.M., Van Geffen, J.H.G.M., Taylor, M., Fountoulakis, I., Koukoulis, M.E., Van Weele, M., Van der A, R.J., Bais, A., Meleti, C. and Balis, D. (2017): TEMIS UV product validation using NILU-UV ground-based measurements in Thessaloniki, Greece, *Atmos. Chem. Phys.*, 17, 7157-7174, <https://doi.org/10.5194/acp-17-7157-2017>

Appendix

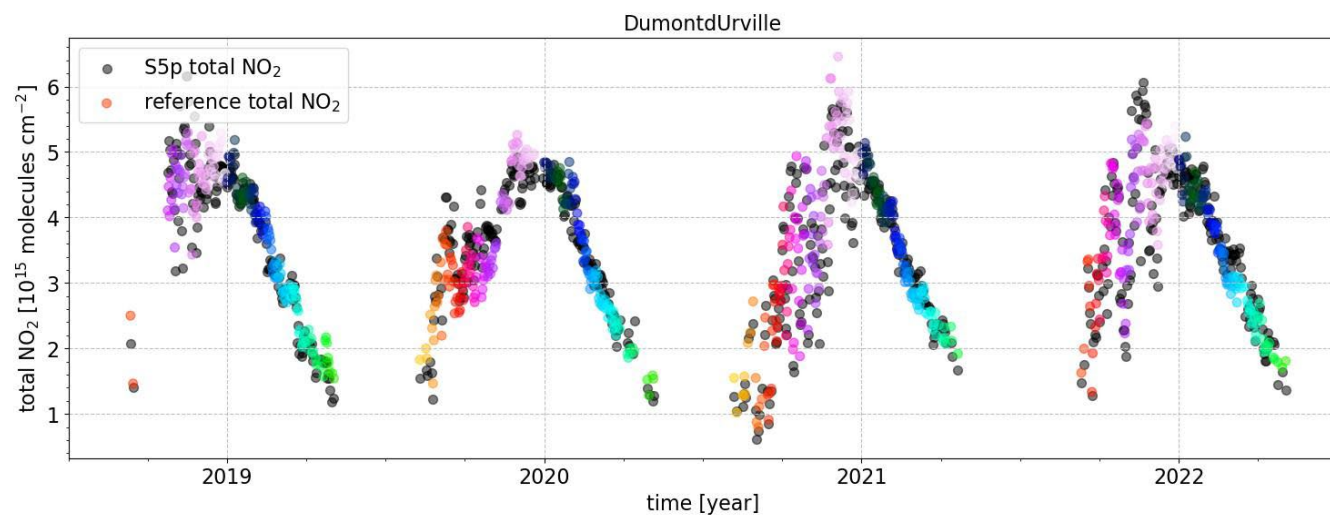


Figure A1.

945 As Figure 1A but color coded according to time of the year (color coding also used in Figure 1B).

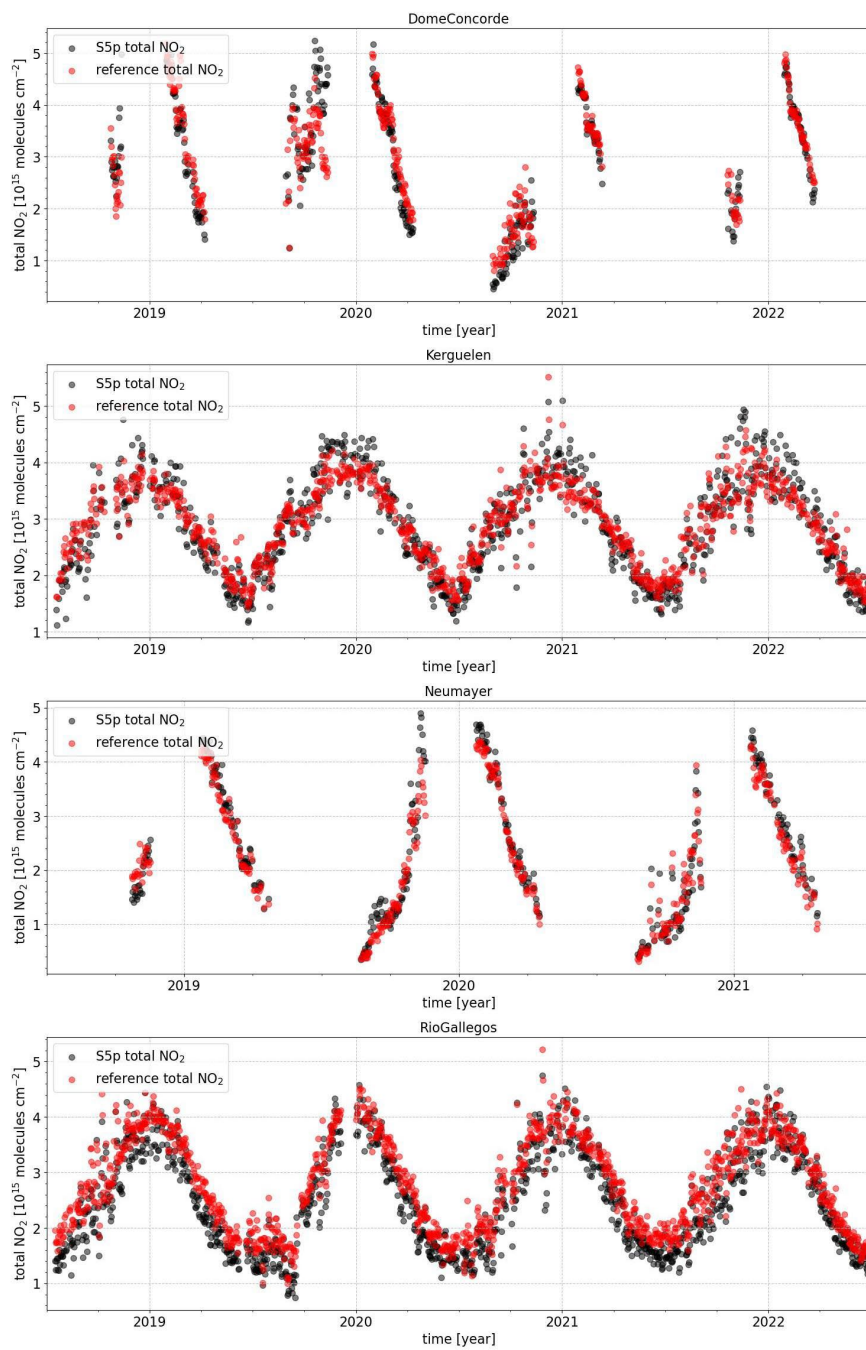
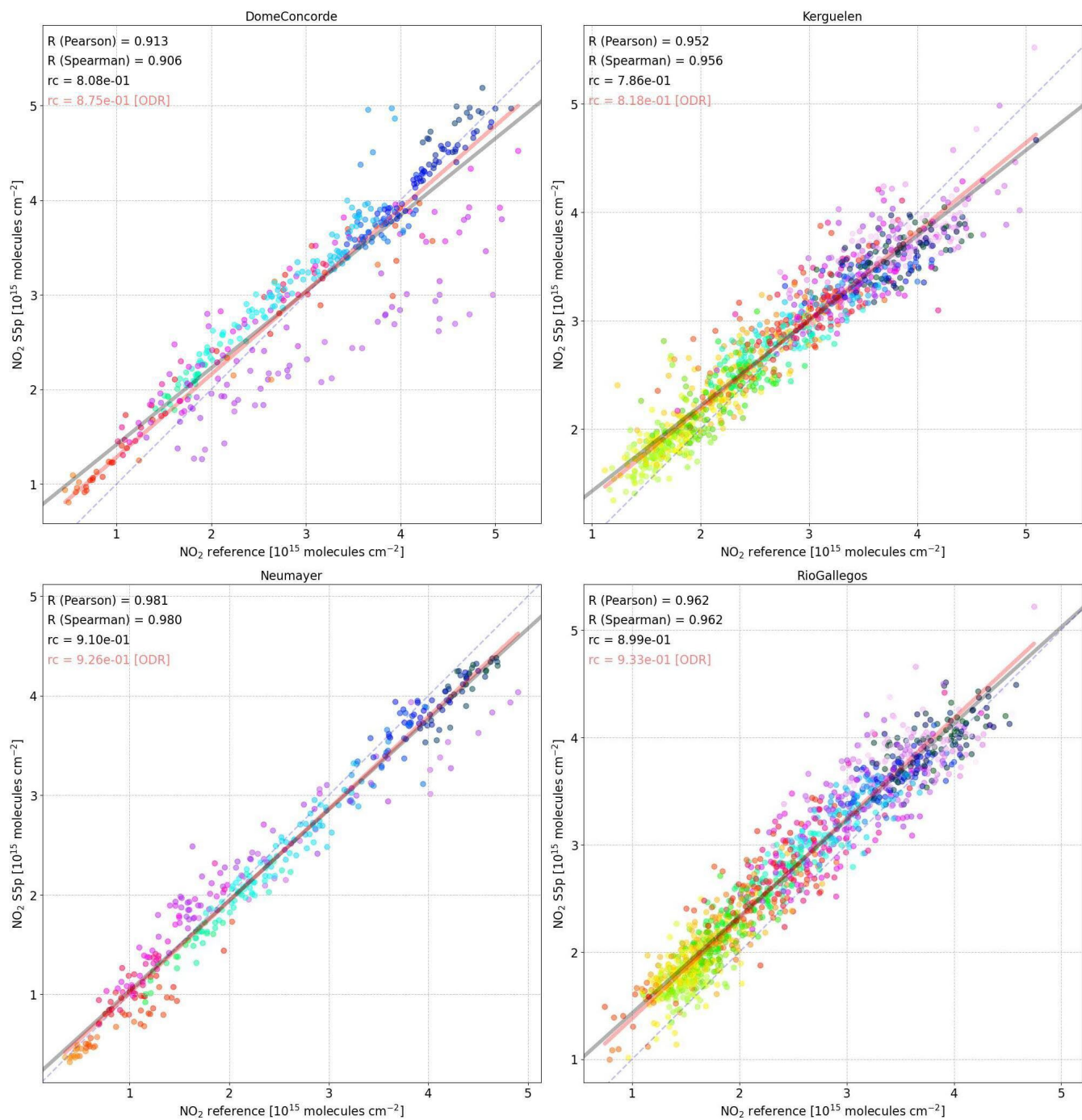


Figure A2A.

As Figure 1A but for the other surface measurement stations in table 1.



950

Figure A2B.

As Figure 1B but for the other surface measurement stations in table 1.

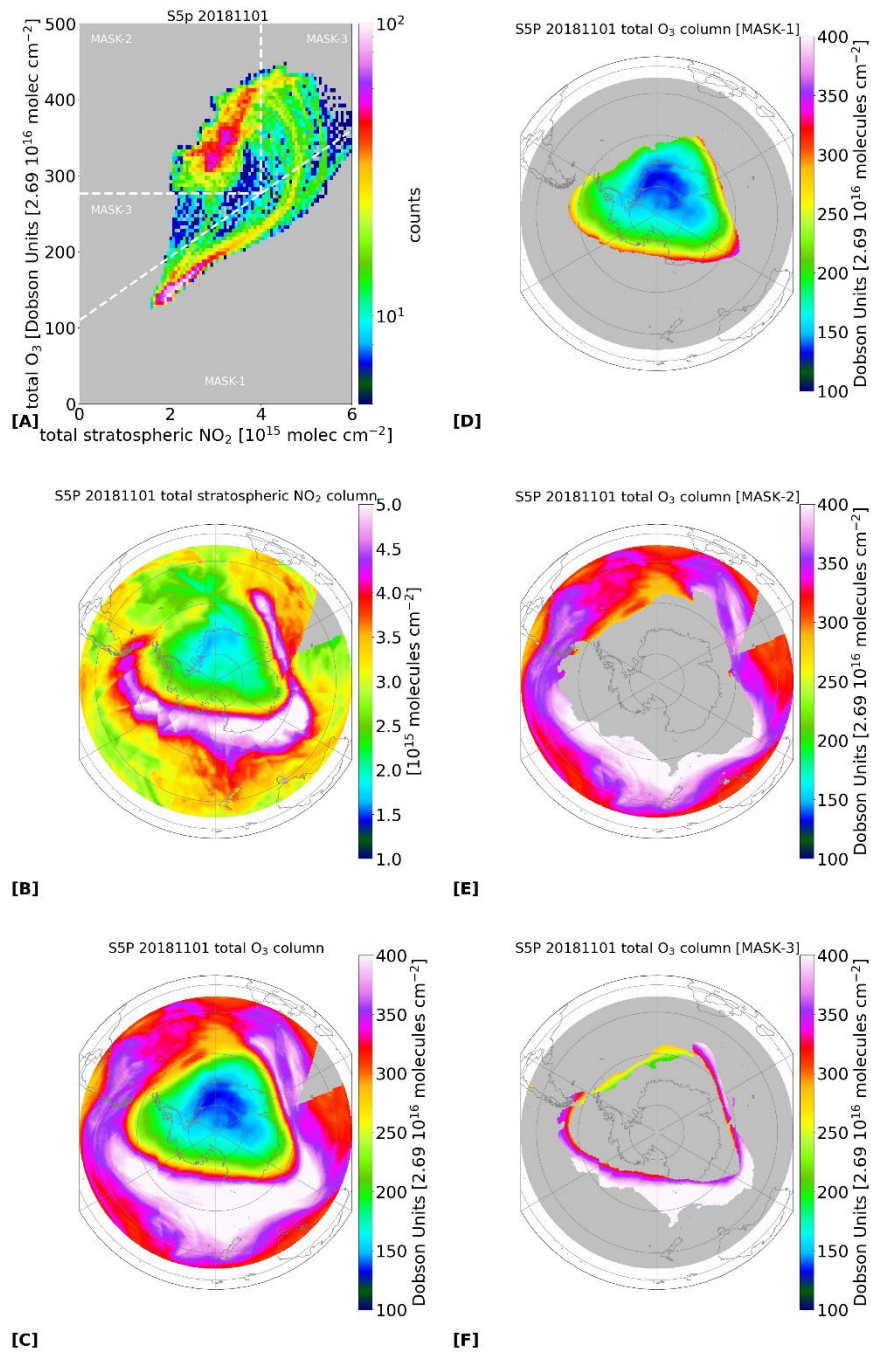


Figure A3.

955 As Figure 5 but for TROPOMI TCO₃ pixel data collocated with TROPOMI SNO₂ pixel data.